

## MIT Open Access Articles

*A wave damping model for flexible marsh plants with leaves considering linear to weakly nonlinear wave conditions*

The MIT Faculty has made this article openly available. **Please share** how this access benefits you. Your story matters.

**Citation:** Zhang, Xiaoxia, Lin, Pengzhi and Nepf, Heidi. 2022. "A wave damping model for flexible marsh plants with leaves considering linear to weakly nonlinear wave conditions." Coastal Engineering, 175.

**As Published:** 10.1016/J.COASTALENG.2022.104124

**Publisher:** Elsevier BV

**Persistent URL:** <https://hdl.handle.net/1721.1/148788>

**Version:** Author's final manuscript: final author's manuscript post peer review, without publisher's formatting or copy editing

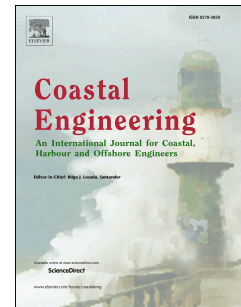
**Terms of use:** Creative Commons Attribution-NonCommercial-NoDerivs License



# Journal Pre-proof

A wave damping model for flexible marsh plants with leaves considering linear to weakly nonlinear wave conditions

Xiaoxia Zhang, Pengzhi Lin, Heidi Nepf



PII: S0378-3839(22)00041-2

DOI: <https://doi.org/10.1016/j.coastaleng.2022.104124>

Reference: CENG 104124

To appear in: *Coastal Engineering*

Received Date: 13 December 2020

Revised Date: 26 October 2021

Accepted Date: 2 April 2022

Please cite this article as: Zhang, X., Lin, P., Nepf, H., A wave damping model for flexible marsh plants with leaves considering linear to weakly nonlinear wave conditions, *Coastal Engineering* (2022), doi: <https://doi.org/10.1016/j.coastaleng.2022.104124>.

This is a PDF file of an article that has undergone enhancements after acceptance, such as the addition of a cover page and metadata, and formatting for readability, but it is not yet the definitive version of record. This version will undergo additional copyediting, typesetting and review before it is published in its final form, but we are providing this version to give early visibility of the article. Please note that, during the production process, errors may be discovered which could affect the content, and all legal disclaimers that apply to the journal pertain.

© 2022 Published by Elsevier B.V.

### **Author credit Statements**

**Xiaoxia Zhang:** Conceptualization, Methodology, Validation, Formal analysis, Investigation, Data curation, Visualization, Writing – review & editing, and Funding acquisition.

**Pengzhi Lin:** Supervision, Conceptualization, and Writing – review & editing.

**Heidi Nepf:** Supervision, Conceptualization, Methodology, Investigation, Formal analysis, Writing – review & editing, and Funding acquisition.

# A wave damping model for flexible marsh plants with leaves considering linear to weakly nonlinear wave conditions

Xiaoxia Zhang<sup>1,2</sup>, Pengzhi Lin<sup>1\*</sup>, and Heidi Nepf<sup>2</sup>

<sup>1</sup> State Key Laboratory of Hydraulics and Mountain River Engineering, Sichuan University, China

<sup>2</sup> Department of Civil and Environmental Engineering, Massachusetts Institute of Technology, USA

\* Email: cvelinpz@scu.edu.cn

## Abstract

Marsh plants protect the coasts and coastal communities by dissipating wave energy. The dissipation of wave energy depends on the geometric (leaf and stem dimensions) and mechanical (material rigidity) properties of the plants. First, flexible plants bend in response to hydrodynamic drag (called reconfiguration), which diminishes wave decay relative to a rigid plant of the same morphology. Second, mutual sheltering between plant leaves and stem can reduce the drag, and thus wave damping. This study connects the prediction of drag on an individual plant and the measurement of wave decay over a meadow of plants to build a physically-based wave-damping model that includes leaves, the impact of reconfiguration, and the impact of sheltering between plant elements. Model plants were constructed to be both geometrically and dynamically similar to *Spartina alterniflora*. The wave damping model assumed linear wave conditions, but was validated using a wide range of weak nonlinear wave conditions within model plants, over a patch of live *Spartina anglica* in the laboratory, and over a meadow of *Spartina alterniflora* in the field. After validation, the model was used to explore the variation in wave decay over a range of wave parameters and plant geometric and bio-mechanic parameters, including stem length, stem diameter, number of leaves per plant, leaf length, leaf width, the rigidity of the stem and the leaf.

**Keywords:** wave damping; salt marsh; flexible plant; drag force; dynamic models

## 1    **1    Introduction**

2    Salt marshes provide many ecosystem services. They are the foundation of food webs, promote  
 3    biodiversity and provide habitat and food for marine species (Barbier et al., 2011). They  
 4    accumulate and store carbon stocks (called blue carbon) at rates that exceed terrestrial forests  
 5    (Mcleod et al., 2011; Pendleton et al., 2012). They protect against coastal flooding by dissipating  
 6    wave energy and reducing storm surge (Arkema et al., 2017; Schoutens et al., 2020). A recent  
 7    study revealed that salt marshes, when combined with engineered defenses, can lower the flood  
 8    magnitude by confining breach size in the engineered defenses (Zhu et al., 2020). By dissipating  
 9    wave energy, marshes promote sedimentation that maintains coastal elevation (Elschot et al.,  
 10    2013). Further, the hibernating roots of marsh plants assure low erosion rates even in winter, when  
 11    the aboveground biomass is decayed or washed away (Schoutens et al., 2019). By promoting  
 12    sedimentation and reducing erosion, marshes can mitigate the impact of sea-level rise on the  
 13    coastline (Duarte et al., 2013). Based on the several ecosystem services they provide, marshes are  
 14    recommended as a nature-based solution for coastal protection (Sutton-Grier et al., 2015).

15        The material rigidity of a marsh plant can facilitate its survival by reducing hydrodynamic  
 16    drag. For example, marsh plants have a lower flexural rigidity at sites with greater wave exposure  
 17    (Cao et al., 2020), which allows them to reconfigure, decreasing the wave drag (Silinski et al.,  
 18    2015). The wave forces on stiff plants can be three times higher than that on flexible plants (e.g.,  
 19    Paul et al., 2012; Bouma et al., 2005). The reduction in wave force associated with plant motion  
 20    also decreases the wave dissipation that can be achieved by the meadow, compared to rigid plants  
 21    with the same morphology and meadow density (Paul et al. 2012; Tan et al., 2019; van Veelen et  
 22    al., 2020). Further, both the leaves and the stem contribute to wave damping (e.g., Heuner et al.,  
 23    2015; Tinoco et al., 2020). In fact, the leaves account for 10% to 90% of the total hydrodynamic  
 24    force on a plant (e.g., Jalonen and Järvelä, 2013; Whittaker et al., 2013; Västilä and Järvelä, 2014;  
 25    Zhang and Nepf, 2020, 2021).

26        Previous studies have empirically quantified wave attenuation using laboratory experiments  
 27    with model plants (e.g., Koftis et al., 2013; Anderson and Smith, 2014) and with live plants (e.g.,  
 28    Maza et al., 2015; Wang et al., 2016), as well as through field surveys (e.g., Knutson et al., 1982;  
 29    Moeller et al., 1996; Yang et al., 2012; Rupprecht et al., 2015; Foster-Martinez et al., 2018; Garzon

et al., 2019). While many of these studies recognize the role of leaves and plant flexibility on wave attenuation, these attributes are usually neglected in wave damping models (e.g., Dalrymple et al., 1984; Mendez and Losada, 2004). Specifically, most previous studies represent marsh plants as rigid cylinders with a diameter equal to the stem diameter, and fit an empirical drag coefficient to this cylinder model. A summary of these fitted drag coefficients is provided in Vuik et al. (2016). However, these fitted drag coefficients cannot be applied with confidence to other sites, because the influence of several plant properties (rigidity and leaf number and geometry) are lumped-into the bulk drag coefficient.

A few studies have explicitly modeled the drag reduction of a simple flexible structure, e.g., a flat blade or a circular cylinder, due to wave-induced motion (e.g., Mullarney and Henderson, 2010; Luhar and Nepf, 2016; Paul et al., 2016; Wan et al., 2017). Specifically, the motion of and drag on the plant element are governed by three dimensionless parameters (Luhar and Nepf, 2016): the Buoyancy number  $B$ , is the ratio of the restoring forces due to buoyancy and stiffness, the wave Cauchy number  $Ca$ , is the ratio of the hydrodynamic drag to the restoring force due to stiffness, and the length ratio  $L$ , is the ratio of element length to the wave excursion,

$$B = \frac{\Delta\rho g V_p}{EI/l^2} \quad (1)$$

$$Ca = \frac{\rho A U_w^2}{EI/l^2} \quad (2)$$

$$L = \frac{l}{A_w} \quad (3)$$

in which  $\Delta\rho$  is the density difference between water ( $\rho$ ) and plant ( $\rho_p$ ).  $g$  is the gravitational acceleration,  $V_p$  is the volume of the plant element (leaf or stem),  $E$  is the elastic modulus and  $I$  is the second momentum of area,  $l$  is the length and  $A$  is the frontal area of the plant element.  $U_w$  is the maximum horizontal wave orbital velocity,  $A_w = U_w/\omega = U_w T_w/(2\pi)$  is the wave orbital excursion,  $\omega$  is the wave angular frequency and  $T_w$  is the wave period.

For marsh plants with both leaves and stem, the dimensionless parameters (Eqs. 1 to 3) can be defined for the leaf ( $B_l, Ca_l, L_l$ ) and stem ( $B_s, Ca_s, L_s$ ), indicated with a subscript  $l$  and  $s$ , respectively, using the corresponding dimensions and rigidity. The plant geometric and mechanical properties for five marsh species are listed in Table 1, from which  $B$ ,  $Ca$ , and  $L$  have been estimated for  $U_w = 0.1$  to  $0.6$  m/s (Garzon et al., 2019; Yang et al., 2020) and  $T_w = 1$  to  $5$  s

(Jadhav and Chen, 2013; Vuik et al., 2016; Zhang et al., 2020), representing a wide range of wave conditions in the coastal region. Reconfiguration occurs when  $Ca > 1$ . Among all five species, the leaves reconfigure in response to typical wave forces ( $5 \leq Ca_l \leq 2600$ ), but the stems, with greater rigidity, have less tendency to reconfigure ( $0.2 \leq Ca_s \leq 250$ ). Once a plant element is in motion ( $Ca > 1$ ), the length ratio ( $0.2 \leq L \leq 220$ , Table 1) indicates whether the plant can follow the wave motion ( $L > 1$ ) or not ( $L < 1$ ), which affect the relative velocity between the fluid and the plant elements (Luhar and Nepf, 2016; Lei and Nepf, 2019b). Finally, the buoyancy parameter,  $B$ , is estimated to have an upper limit of 0.07 to 7 (Table 1). This range of  $B$  only slightly affect the plant motion (Luhar and Nepf, 2011) and has negligible influence on the measured wave-force on the plant (Luhar and Nepf, 2016), and the effect of the Buoyancy number will not be discussed in this study.

A reconfiguration model for an individual simple structure (Mullarney and Henderson, 2010; Gosselin et al., 2010; Luhar and Nepf, 2016) was successfully applied to predict the wave decay over a meadow of model seagrass (Luhar et al., 2017) and live seagrass in the field (Lei and Nepf, 2019a), as well as live marsh plants (van Veelen et al., 2021), and each of these studies highlighted the importance of plant flexibility on wave damping. For marsh plants with both leaves and stem, Zhang and Nepf (2021) proposed a model for drag on a marsh plant that incorporated the reconfiguration of both leaves and stem as well as the sheltering between leaves and stem. In the present study, the wave-energy dissipation by a meadow of marsh plants with flexible leaves and stem was predicted using the force on individual plants and validated against laboratory experiments using model plants (the present study) and live plants (Maza et al., 2015; Lara et al., 2016; Losada et al., 2016) as well as marshes in the field (Garzon et al., 2019). Once validated, the model was used in a systematical analysis of the influence on wave dissipation due to each of the plant and wave parameters. Specifically, wave decay was modeled under a wide range of water depth, wave amplitude, and wave period, stem length ( $l_s$ ), diameter ( $D$ ), and rigidity ( $E_s I_s$ ), as well as the number of leaves per plant ( $N_l$ ), leaf length ( $l_l$ ), width ( $b$ ), and rigidity ( $E_l I_l$ ), covering a wide range of dimensionless parameters in the field (Table 1). The predictions and scale analysis illustrated the physical mechanisms linking plant and wave properties to wave dissipation.

**Table 1.** Plant parameters for five marsh species: *Phragmites australis*, *Scirpus maritimus*, *Scirpus tabernaemontani*, *Spartina alterniflora*, and *Spartina anglica*.  $N_s$  and  $N_l$  are the number of stems per unit bed area and the number of leaves per stem, respectively.  $B$ ,  $Ca$ , and  $L$  were estimated with plant density  $\rho_p = 840 \text{ kg/m}^3$ , which is the lower value reported for *Spartina alterniflora* (Zhang and Nepf, 2021) wave orbital velocity  $U_w = 0.1$  to  $0.6 \text{ m/s}$ , and wave period  $T_w = 1$  to  $5 \text{ s}$ , which are typical values for coastal region.  $E_l = 3 \text{ GPa}$  measured for live *Spartina alterniflora* specimen Zhang and Nepf (2021) was applied for all species due to the lack of leaf elastic modulus data.  $d$  is the leaf thickness.  $KC$  is the Keulegan and Carpenter number, defined by the stem diameter ( $KC_s = U_w T_w / D$ ) and leaf width ( $KC_l = U_w T_w / b$ ), respectively.

parameters	<i>P. australis</i> <sup>[1-6]</sup>	<i>S. maritimus</i> <sup>[7-11]</sup>	<i>S. tabernaemontani</i> <sup>[7,11]</sup>	<i>S. alterniflora</i> <sup>[12-23]</sup>	<i>S. anglica</i> <sup>[9-10, 13, 19, 23-26]</sup>
$N_s \text{ (m}^{-2}\text{)}$	80 to 600	100 to 1000	300 to 800	170 to 420	430 to 880
$N_l \text{ (stem}^{-1}\text{)}$	7 to 18	4 to 8	/	5 to 12	5 to 10
$l_s \text{ (cm)}$	50 to 350	50 to 120	100 to 200	30 to 230	30 to 100
$D \text{ (mm)}$	3 to 15	3 to 9	9 to 15	3 to 10	2 to 8
$l_l \text{ (cm)}$	20 to 40	20 to 40	/	20 to 50	20 to 40
$b \text{ (mm)}$	10 to 30	2 to 12	/	5 to 16	6 to 15
$d \text{ (mm)}$	0.24 to 0.33	0.2 to 0.4	/	0.25 to 0.67	0.2 to 0.47
$E_s \text{ (GPa)}$	5 to 10	0.4 to 1.2	0.12 to 0.13	0.08 to 1.4	0.1 to 0.7
$I_s \text{ (m}^4\text{)}$	$4 \times 10^{-12}$ to $2 \times 10^{-9}$	$4 \times 10^{-12}$ to $3 \times 10^{-10}$	$3 \times 10^{-10}$ to $2 \times 10^{-9}$	$4 \times 10^{-12}$ to $2 \times 10^{-9}$	$8 \times 10^{-13}$ to $2 \times 10^{-10}$
$I_l \text{ (m}^4\text{)}$	$1 \times 10^{-14}$ to $9 \times 10^{-14}$	$1 \times 10^{-15}$ to $6 \times 10^{-14}$	/	$7 \times 10^{-15}$ to $4 \times 10^{-13}$	$4 \times 10^{-15}$ to $1 \times 10^{-13}$
$B_s$	0.07 to 0.5	0.4 to 0.9	3 to 7	0.9 to 2	0.6 to 1.7
$B_l$	0.9 to 4	1 to 2	/	0.8 to 2	1.2 to 2
$Ca_s$	0.2 to 9	0.4 to 90	2 to 130	2 to 90	0.6 to 250
$Ca_l$	23 to 2600	40 to 1400	/	17 to 740	25 to 1440
$L_s$	1 to 220	1 to 75	2 to 130	0.6 to 140	0.6 to 63
$L_l$	0.4 to 25	0.4 to 25	/	0.4 to 31	0.4 to 25
$B_s/Ca_s$	0.01 to 2.3	0.01 to 1.4	0.04 to 2.3	0.01 to 1.5	0.01 to 1.2
$B_l/Ca_l$	0.001 to 0.06	0.001 to 0.08	/	0.001 to 0.1	0.001 to 0.09
$KC_s$	7 to 1000	11 to 1000	7 to 330	10 to 1000	13 to 1500
$KC_l$	3 to 300	8 to 1500		6 to 600	7 to 500

Data sources used to estimate the range of plant parameters were marked upright to the species name, where the corresponding references are Ostendorp and Möller (1991)<sup>[1]</sup>, Boar et al. (1999)<sup>[2]</sup>, Nada et al. (2015)<sup>[3]</sup>, Cho et al. (2017)<sup>[4]</sup>, Xi et al. (2017)<sup>[5]</sup>, Schaefer (2019)<sup>[6]</sup>, Heuner et al. (2015)<sup>[7]</sup>, Silinski et al. (2015)<sup>[8]</sup>, Vuik et al. (2016)<sup>[9]</sup>, Vuik et al. (2018)<sup>[10]</sup>, Schoutens et al. (2020)<sup>[11]</sup>, Knutson et al. (1982)<sup>[12]</sup>, Zhi et al. (2007)<sup>[13]</sup>, Feagin et al. (2011)<sup>[14]</sup>, Yang et al. (2012)<sup>[15]</sup>, Ysebaert et al. (2011)<sup>[16]</sup>, Jadhav and Chen (2013)<sup>[17]</sup>, Wu et al. (2016)<sup>[18]</sup>, Rupprecht (2015)<sup>[19]</sup>, Zhang and Nepf (2021)<sup>[20]</sup>, Chatagnier (2012)<sup>[21]</sup>, Garzon et al. (2019)<sup>[22]</sup>, Maricle et al. (2009)<sup>[23]</sup>, Li et al. (2009)<sup>[24]</sup>, Li et al. (2011)<sup>[25]</sup>, Losada et al. (2016)<sup>[26]</sup>.

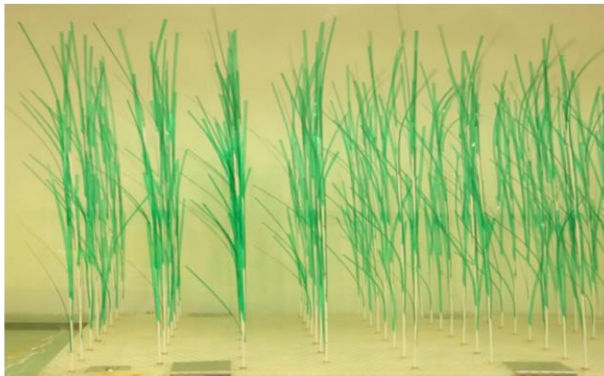


## 2 Laboratory experiments

The model plant was geometrically (1:5) and dynamically similar to *Spartina alterniflora*, as described in Zhang and Nepf (2021). Note that a 1:5 scale was chosen based on the *Spartina alterniflora* leaf and stem measured in the field (Zhang et al., 2020) and to fit the size of the flume. Model plants consisted of ten identical leaves distributed uniformly both along and around the circumference of a central stem (Fig. 1). The stem was 2 mm in diameter and 20 cm long. The leaves were 0.12 mm thick, 3 mm wide, and 10 cm long. The material density for the leaf and stem were 1.35 and 1.06 g/cm<sup>3</sup>, respectively (Table 2). The plant rigidity was tested on an Instron 5965 (Norwood, MA) applying the three-point bending test. The standard deviation of the model leaf (7 tests) and model stem (8 tests) indicated the uncertainty of the method was less than 5%. The elastic modulus was obtained by dividing  $EI$  by  $I$  (Table 2).

Short wood cylinders with 2 mm holes in their center were used to hold the model plants in the baseboard (Fig. 1a). The wooden cylinders expanded after being submerged in water and held the model plants tightly in the holes of the baseboard. Once installed, the wooden cylinders did not extend above the baseboard. The model plants were arranged in a staggered array as shown in Fig. 1b. Once inserted, the erect plants were 30-cm tall. The plants were distributed across the entire flume width and over a streamwise distance of 3.8 m. The plant density was 280 plants/m<sup>2</sup>, which is similar to *Spartina alterniflora* in the field (e.g., Zhang et al., 2020, 173 plants/m<sup>2</sup>; Ysebaert et al., 2011, 330 plants/m<sup>2</sup>).

a) Model marsh plants



b) Arrangement of model plants

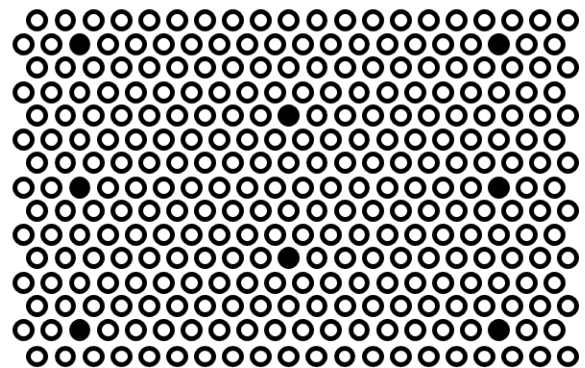


**Fig. 1.** a) Model plants in channel and b) top view of the baseboard with staggered holes (circles) and the plant positions within the hole array (filled circles).

**Table 2.** Material properties of the model plants and the wave conditions tested

Plant properties	$h$ (cm)	$T_w$ (s)	$\lambda$ (m)	$a_w \pm 0.1$ (cm)	$U_w \pm 1$ (cm/s)
$\rho_{p,\text{leaf}} = 1.35 \pm 0.06$ (g/cm <sup>3</sup> )	45	2.0	3.88	1, 1.5, 2.2, 3, 4.1	4, 7, 10, 13, 18
$\rho_{p,\text{stem}} = 1.06 \pm 0.01$ (g/cm <sup>3</sup> )	45	1.4	2.56	1, 1.5, 2.2, 3, 4.1	4, 6, 9, 12, 16
$l_l = 10$ cm	45	1.1	1.77	1, 1.5, 2.2, 3, 4.1	3, 5, 8, 11, 15
$b = 3$ mm, $d = 0.12$ mm	40	1.4	2.46	1, 1.5, 2.2, 3, 4.1	4, 6, 9, 12, 17
$l_s = 20$ cm, $D = 2$ mm	36	1.4	2.36	1, 1.5, 2.2, 3, 4.1	4, 7, 10, 13, 18
$E_l = 4.8 \pm 0.4$ GPa	27	1.4	2.12	1, 1.5, 2.2, 3, 4.1	5, 8, 12, 16, 20
$E_s = 1.72 \pm 0.03$ GPa	18	1.4	1.78	1, 1.5, 2.2	8, 11, 16

The experiments were conducted in a 24-m-long, 38-cm-wide, 60-cm-tall wave channel in the Nepf Fluid Mechanics Lab at MIT (Fig. 2). Monochromatic waves were generated with a piston-type wavemaker. A detailed description is given in the Appendix A in Luhar (2012). A beach with 1:5 slope and covered with a 10-cm thick coconut fiber reduced the wave reflection to  $7\% \pm 3\%$  for the tested wave conditions. Five water depths, 18, 27, 36, 40, and 45 cm were tested, ranging from emergent to submerged. Three wave periods and five wave amplitudes were tested, producing a range of wave length and wave orbital velocity (Table 2). The range of experimental conditions were chosen to have Cauchy numbers that fell within the field conditions, because the Cauchy number defines the dynamic similarity. In addition, the length ratio  $L$ , describing the ratio of plant scale to wave scale, defines the wave kinematic similarity. The dimensionless parameters spanned the following ranges, which overlapped with typical field conditions (Table 1):  $0.01 \leq Ca_s \leq 0.6$ ,  $3.8 \leq L_s \leq 44$ ,  $0.9 \leq Ca_l \leq 75$ ,  $1.9 \leq L_l \leq 22$  (see Table S1 in the Supplementary Material).

At each wave condition, two wave gages were synchronized to measure the free surface displacement at a reference position 4-m upstream of the meadow (wave gauge 1) and at a mobile position along the meadow. During each experiment run (about 90 min), the wave amplitude at wave gage 1 varied by less than 3%, confirming stationary wave conditions. The average wave amplitude measured by wave gage 1 is listed in Table 2. Wave gage 2 collected data at 10 and 15 cm intervals along the meadow, depending on the wavelength. At each position, the free surface displacement,  $\eta(t)$ , was recorded at 2000 Hz for 1 min. Additional measurements of wave amplitude were made without plants to assess the wave decay associated with the channel wall and baseboards alone.

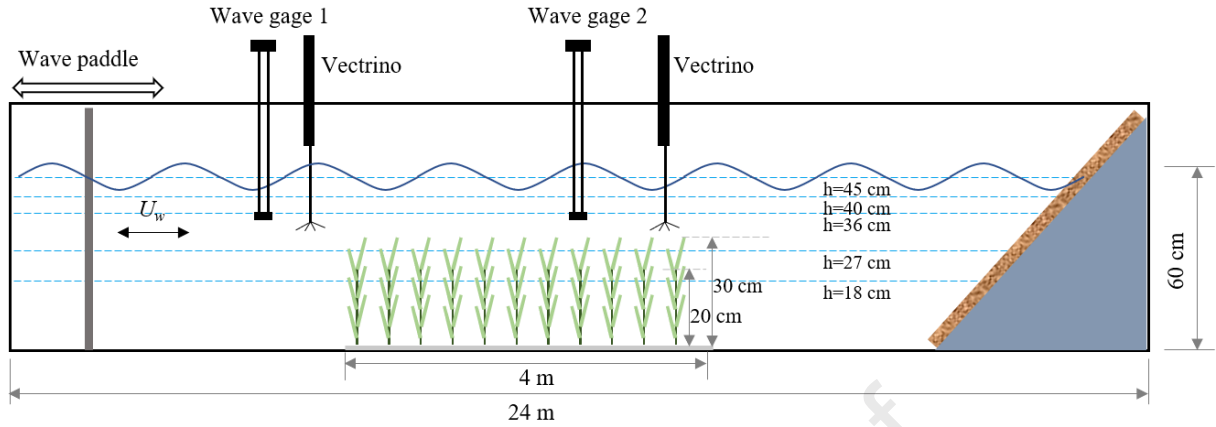


**Fig. 2.** Schematic of the experiment, not to scale. The wave paddle is located at the left in the figure. A beach with 1:5 slope and covered with a 10-cm thick layer of coconut fiber was located at the downstream end to reduce wave reflection. The model meadow was located at mid-length along the flume. Two wave gages measured the wave height at a reference position (wave gage 1) and along the meadow (wave gage 2). Velocity in front and at the end of the meadow was measured by Vectrino+.

For each surface displacement record, the angular frequency  $\omega = 2\pi/T_w$  was determined by Fourier fitting using the cftool in MATLAB. For sampling frequency  $f_s$ , there were  $\gamma = 2\pi/\omega f_s$  samples and thus  $\gamma$  phase bins in each wave period (Lei and Nepf, 2019a). For sample duration  $\Delta t$ , each record contained  $M = \Delta t/T_w$  wave periods. The phase averaged surface displacement in the  $n^{\text{th}}$  phase bin ( $n = 1$  to  $\gamma$ ), corresponding to phase  $\phi = 2\pi n/\gamma$  was determined by,

$$\hat{\eta}(\phi(n)) = \frac{1}{M} \sum_{m=0}^{M-1} \eta(n + \gamma m) \quad (4)$$

The wave amplitude  $a_w$  was calculated from the root-mean-square of the phase-averaged surface displacement,

$$a_w = \sqrt{\frac{2}{\gamma} \sum_{n=1}^{\gamma} \hat{\eta}^2(\phi(n))} \quad (5)$$

Fig. 3 shows an example of wave amplitude measured along the meadow (circles) for  $h=45$  cm,  $T_w = 1.4$  s, and  $a_w = 4$  cm. The measured wave amplitude was the sum of the incoming wave and the beach-reflected wave, resulting in an amplitude modulation at an interval of  $\lambda/2$ . A fitting method was developed to account for this modulation. Specifically, Eq. S9 in Lei and Nepf (2019a) was rearranged and used to fit the measured wave amplitude including the beat pattern along the meadow,

$$\frac{1}{a_{w,x}} = K_D x + C_1 \cos(2kx + \epsilon) + C_2 \quad (6)$$

in which  $k = 2\pi/\lambda$  is the wavenumber,  $K_D$ ,  $\epsilon$ ,  $C_1$ , and  $C_2$  are fitting coefficients. Examples of the fitting are shown as curves in Fig. 3 for the same wave conditions with vegetation ( $K_{D,T} = 0.92 \pm 0.04 \text{ m}^{-2}$  with 95% CI) and without vegetation ( $K_{D,b} = 0.28 \pm 0.04 \text{ m}^{-2}$ ). Finally, the wave decay coefficient attribute to the plants was obtained by the difference,  $K_D = K_{D,T} - K_{D,b}$  ( $= 0.64 \pm 0.06 \text{ m}^{-2}$  for the case shown in Fig. 3). The wave decay coefficients attributed only to the plants,  $K_D$ , are discussed below and are summarized in Table S1 in the Supplementary Material. The wave amplitude along the channel with and without plants is shown in Appendix C.

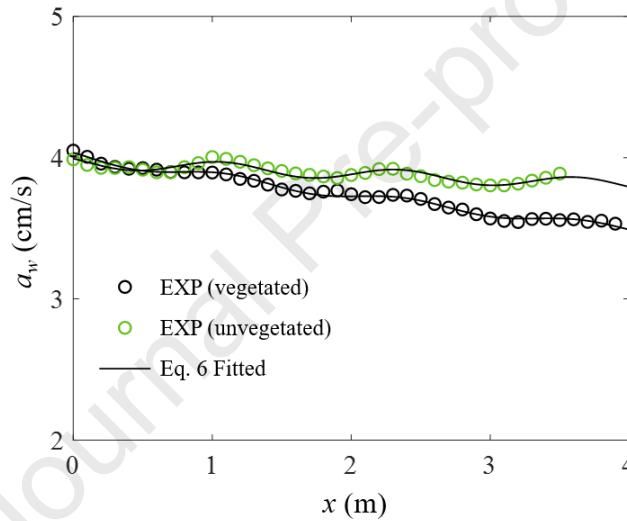


**Fig. 3.** The wave amplitude as a function of distance along the meadow for test conditions  $h = 40$  cm,  $T_w = 1.4$  s, and  $a_w = 4.1$  cm. black and green circles correspond to experiments with and without the model vegetation. Based on the fitted wave amplitude evolution along the meadow (Eq. 6, solid curves),  $K_{D,T} = 0.92 \pm 0.04 \text{ m}^{-2}$  (95% CI) and  $K_{D,b} = 0.28 \pm 0.04 \text{ m}^{-2}$  for the channel with vegetation and the channel without vegetation, respectively.

Two Nortek Vectrino+ were used to measure the velocity profiles with 1 to 2 cm vertical resolution at the leading and trailing edge of the meadow (Fig. 2). At each measurement point, the Vectrino+ recorded a 1-min record with a sampling frequency of 200 Hz. Each velocity measurement was quality checked by the signal to noise ratio. Each velocity record was separated into phase bins and de-spiked within each phase bin using the methods described in Goring and Nikora (2002) and Nikora and Goring (2000). The phase averaged velocity  $\hat{u}(\phi(n))$  was defined

similarly to Eq. 4 after de-spiking. The measured wave orbital velocity was represented by the root-mean-square of the phase-averaged velocity,  $u_w = \sqrt{\frac{2}{\gamma} \sum_{n=1}^{\gamma} \hat{u}^2(\phi(n))}$ , and the depth-averaged wave velocity over the submerged portion of the undeflected plant ( $h_p = \min(h, l_s + l_l)$ ) was  $U_w = \frac{1}{h_p} \int_0^{h_p} u_w(z) dz$ . The value of  $U_w$  at the leading edge of the meadow is given in Table 2 and the velocity profiles  $u_w$  were summarized in table S2.

### 3 Numerical prediction of wave damping

#### 3.1 Force on an individual plant

Zhang and Nepf (2021) developed a model to predict the wave-induced reconfiguration of and drag on an individual marsh plant with flexible leaves and stem. The plant has  $N_l$  identical leaves (length  $l_l$ , width  $b$ , thickness  $d$ ) distributed both along and around the stem (stem length  $l_s$  and diameter  $D$ ). The plant material density  $\rho_p$ , elastic modulus for the leaves  $E_l$  and for the stem  $E_s$  are all constants. The mathematical description of the motion of and force on a representative leaf with a vertical orientation and the stem with leaves attached are given in Zhang and Nepf (2021), but repeated here for convenience,

$$\frac{\partial}{\partial s}((V + iT)e^{-i\theta}) + if_B + (f_D + if_F + f_{AM})e^{-i\theta} + f_{VB} + f_l = \rho_p A_c \frac{\partial^2 \tilde{x}}{\partial t^2} \quad (7)$$

in which the location of each position ( $s$ ) along the element is described by the streamwise ( $x$ ) and vertical ( $z$ ):  $\tilde{x} = x(s) + iz(s) = \int_0^s i e^{-i\theta} ds' = \int_0^s \sin\theta ds' + i \int_0^s \cos\theta ds'$ , with  $s'$  a dummy variable, and  $\theta$  the local angle between the plant element and vertical. The fluid forces per unit length include the buoyancy force  $f_B$ , the drag force  $f_D$ , the skin friction  $f_F$ , the added mass force  $f_{AM}$ , and the Froude-Krylov (virtual buoyancy) force  $f_{VB}$ . For the stem,  $f_l$  is the distributed force associated with the drag on all the leaves. Under these external forces the plant element experiences a shear force  $V = -\partial(EI\partial\theta/\partial s)/\partial s$  and tension  $T$ . The unsteady motion of the plant generated an inertial force term,  $\rho_p A_c \frac{\partial^2 \tilde{x}}{\partial t^2}$ , with  $A_c$  the cross-sectional area.

To predict the drag on the full marsh plant, Eq. 7 was first applied to a vertical leaf with  $f_l = 0$  to obtain the shear ( $V_l$ ) and tension ( $T_l$ ) for one representative leaf. Second, Eq. 7 was applied to the stem to obtain the stem motion and the total horizontal shear force  $V_{s0}$  and vertical tension

$T_{s0}$  on the stem, which represented the total force on the full plant. The distributed force on the stem due to all the leaves is  $f_l = (C_s N_l (-V_{l0} - iT_{l0}))/l_s$ , in which  $V_{l0}$  and  $T_{l0}$  are the shear force and tension at the base of the representative leaf. The sheltering coefficient,  $C_s$  ( $0 \leq C_s \leq 1$ ) describes the reduction in drag on individual leaves due to sheltering between the leaves and the stem, and  $C_s = 1$  indicates no sheltering. The sheltering coefficient  $C_s = 0.6$  (Zhang and Nepf, 2021) was applied in this study. The drag coefficient  $C_D$  and the inertial coefficient  $C_M$  for the leaf and stem, are functions of the Keulegan and Carpenter number ( $KC$ ) and depend on the plant scale. For the cylindrical stem of diameter  $D$ ,  $KC_s = U_w T_w / D$ . For the flat leaf of width  $b$ ,  $KC_l = U_w T_w / b$ . The drag and inertial coefficients for a rigid cylinder and slat were used for the stem and leaf, respectively (Keulegan and Carpenter, 1958) and are summarized in the Appendix A. For more details about the model, please see Zhang and Nepf (2021).

### 3.2 Wave damping by a meadow of plants

The force on an individual plant can be used to estimate the wave-energy dissipation generated by a meadow of plants. Assuming linear wave theory, the wave-energy dissipation caused by the vegetation can be described by the steady wave energy balance,

$$-E_D = \frac{\partial(\frac{1}{2}\rho g a_w^2 C_g)}{\partial x} \quad (8)$$

in which  $E_D$  is the spatial rate of wave energy dissipation, which was assumed here to be associated only with the plants.  $C_g$  is the wave group velocity. Within the meadow, it is usually assumed that the work done by the vertical force component is much smaller than that by the horizontal force (Mendez and Losada, 2004), so that only the horizontal force on the plant,  $F_d = -V_{s0}$ , is considered. Assuming the force on each plant is independent, i.e., no interaction among plants, the rate of wave energy dissipation equals the work done by plants on the flow.

$$E_D = E_{plant} = \frac{1}{T_w} \int_{t=0}^{T_w} N_s F_d \tilde{u} dt \quad (9)$$

in which  $N_s$  is the number of plants per unit bed area. The assumption of no interaction among plants is reasonable for sparse meadows, e.g., the plant density reported by Xi et al. (2017) (87 to 140 plants/m<sup>2</sup>) and Cho et al. (2017) (80 to 200 plants/m<sup>2</sup>) for *Phragmites australis*, and by Zhang et al. (2020) (173 plants/m<sup>2</sup>) for *Spartina alterniflora*. For dense meadows, the wave damping can be predicted by the force model for individual flexible plants using the in-canopy velocity, based



on Hu et al. (2014), Lei and Nepf (2019a), and van Veelen et al. (2021).

As the wave amplitude changes along the meadow, the plant force and the energy dissipation also change. Therefore, the wave amplitude along the meadow needs to be predicted by the marching method illustrated in Fig. 4, with a step length  $dx$ .

$$a_{w,ndx} = \sqrt{a_{w,(n-1)dx}^2 - \frac{E_D dx}{1/2 \rho g C_g}} \quad (10)$$

in which  $a_{w,ndx}$  is the wave amplitude at  $x = ndx$  from the leading edge of the meadow in the direction of wave propagation. For an incoming wave  $a_{w,0}$  at the marsh edge  $x = 0$ , the wave amplitude at each location  $x = ndx$ ,  $n = 1:N$ , was estimated in sequence using the following steps, and with  $n = 0$  at the marsh edge.

- 1) Estimate the wave orbital velocity  $\tilde{u}(= u_x + iu_z)$  at  $x = (n-1)dx$  using linear wave theory. Here, the depth averaged wave orbital velocity over the submerged plant height  $h_p$  was used,

$$\begin{aligned} u_x &= \frac{1}{h_p} \int_{-h}^{h_p-h} a_{w,x} \omega \frac{\cosh k(h+z)}{\sinh kh} \sin(\omega t) dz \\ u_z &= \frac{1}{h_p} \int_{-h}^{h_p-h} a_{w,x} \omega \frac{\sinh k(h+z)}{\sinh kh} \cos(\omega t) dz \end{aligned} \quad (11)$$

- 2) Use the  $KC$  number for the leaf  $KC_l$  and the stem  $KC_s$  to determine the drag coefficient and inertia coefficient for the leaf ( $C_{D,l}$ ,  $C_{M,l}$ ) and the stem ( $C_{D,s}$ ,  $C_{M,s}$ ) as summarized in the Appendix A. Estimate the wave orbital excursion  $A_w$  and the dimensionless parameters for the leaf (e.g.,  $Ca_l$ ,  $L_l$ ) and the stem (e.g.,  $Ca_s$ ,  $L_s$ ).
- 3) Predict the time-varying total force  $F_d = -V_{s0}$  on an individual plant using Eq. 7 with the plant and wave parameters calculated in step 1 and step 2.
- 4) Use  $F_d(t)$  in Eq. 9 to obtain the wave energy dissipation rate  $E_D$ .
- 5) Substitute  $E_D$  into Eq. 10 to obtain the wave amplitude  $a_{w,ndx}$  at  $x = ndx$ .
- 6) Repeat step 1 to step 5 through to  $n = N$ .

The step size  $dx$  must be decreased until its value no longer impacts the solution. We found that for  $dx \leq \lambda/5$  ( $\lambda$  is the wavelength), the impact of  $dx$  on the solution was reduced to less than 1%. Therefore, all predictions in this study applied a step length  $dx = 0.2$  m, except for the validation using the filed measurements of Garzon et al. (2019), which applied  $dx = 0.5$  m

considering the wave length and the meadow length. The step length  $dx$  is within one fifth of the wave length for all cases, which reduced the impact of  $dx$  on the solution to 1%.

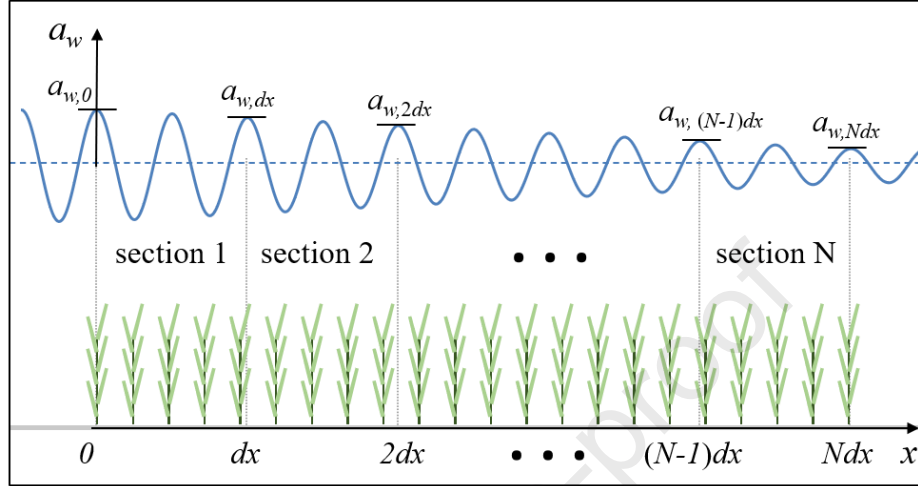


**Fig. 4.** Illustration of the progressive prediction of wave amplitude using wave-induced plant force model. The meadow was divided into  $N$  sections with equal length,  $dx$ , in the direction of wave propagation. Starting from the wave amplitude  $a_{w,0}$  at the marsh edge  $x = 0$ , the wave amplitude along the meadow is estimated by marching the solution forward in space, predicting the wave amplitude at  $x = ndx$  using the wave parameters at  $x = (n - 1)dx$ .

Previous studies have evaluated wave decay using the model derived by Dalrymple et al. (1984) for linear waves propagating through an array of rigid circular cylinders (e.g., Maza et al., 2019; van veelen et al., 2020; Gijón Mancheño et al., 2021),

$$\frac{a_{w,x}}{a_{w,0}} = \frac{1}{1 + K_D a_{w,0} x} \quad (12)$$

in which  $K_D$  is the wave decay coefficient. Eq. (12) can be recast in terms of the incoming wave amplitude  $a_{w,0}$  and the transmitted wave amplitude  $a_{w,Ndx}$ .

$$K_D = \frac{1}{Ndx} (1/a_{w,Ndx} - 1/a_{w,0}) \quad (13)$$

A decay coefficient,  $K_D$ , was estimated by applying Eq. 13 to the amplitude predicted from Eq. 9.

Finally, the wave damping model was derived based on linear wave theory, but cautiously used for weakly nonlinear wave conditions (as in section 4). The nonlinearity of the wave conditions used in the present study was summarized in Appendix B.



## 4 Results and Discussion

### 4.1 Experiment results and model validation

The range of plant motion within the meadow was similar to an isolated plant. For example, for the same wave conditions ( $h = 45$  cm,  $T_w = 2$  s, and  $a_w = 4.1$  cm), the ratio of tip excursion to stem length was 18% in the meadow and 20% for the isolated plant (Fig. 5). In addition, the wave orbital velocity within the meadow followed linear wave theory, i.e., was not transformed by the meadow (measured wave orbital velocities are shown in Appendix B). Based on these observations, it was reasonable to assume that the single plant drag model (Eq. 7) could be used to represent plant drag within a meadow, and thus to predict the wave decay. The predicted wave decay coefficient  $K_D$  had good agreement with the measured wave decay coefficient (Fig. 6). The measured and predicted wave decay coefficient  $K_D$  for each wave conditions tested in this study is summarized in Table S1 in the Supplementary Material. Specifically,  $K_{D-predict} = (0.87 \pm 0.03)K_{D-measured}$  (95% CI). Among all 33 cases, the average deviation was  $15\% \pm 9\%$ , and only three cases had larger than 30% differences between the measurement and prediction. The maximum difference of 35% was for the largest wave in the emergent condition ( $h = 18$  cm,  $T_w = 1.4$  s, and  $a_w = 2.2$  cm). The good agreement between the prediction and measurement validated the model, including the assumption of no interaction between plants, and over the following conditions:  $0.01 \leq Ca_s \leq 0.6$ ,  $3.8 \leq L_s \leq 44$ ,  $0.9 \leq Ca_l \leq 75$ ,  $1.9 \leq L_l \leq 22$ .

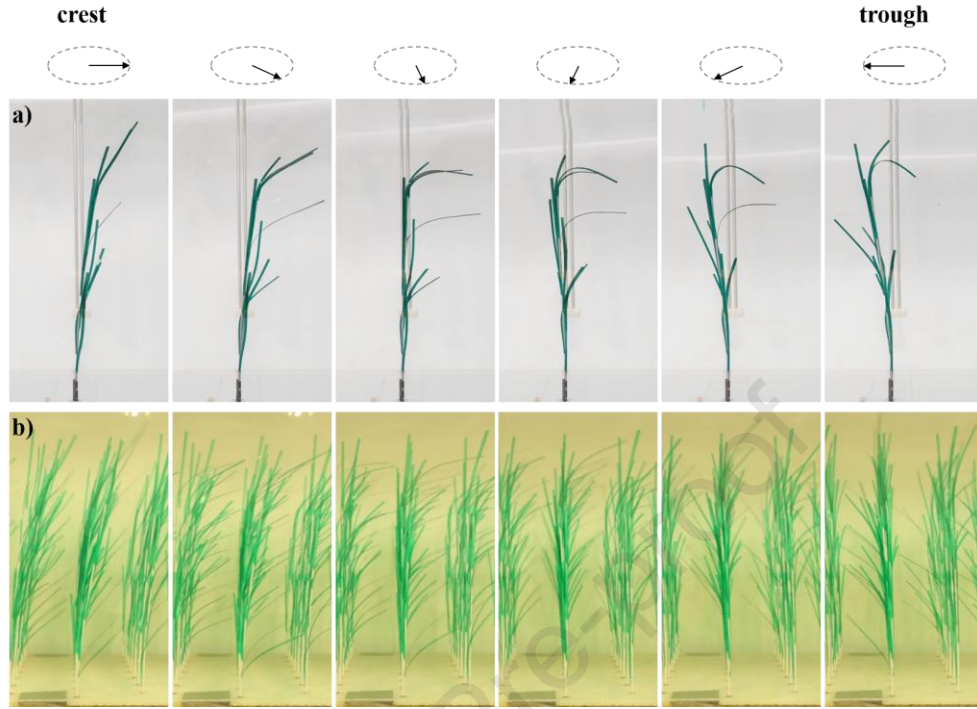


**Fig. 5.** (a) The motion of a single plant (Fig. 5 in Zhang and Nepf, 2021) compared to (b) the plant motion within the meadow for  $h = 45$  cm,  $T_w = 2$  s, and  $a_w = 4.1$  cm. From left to right, the wave went from crest to trough with 0.2 s time interval. The dashed oval illustrates the full wave orbital, with individual arrows showing the wave velocity vector for each image.

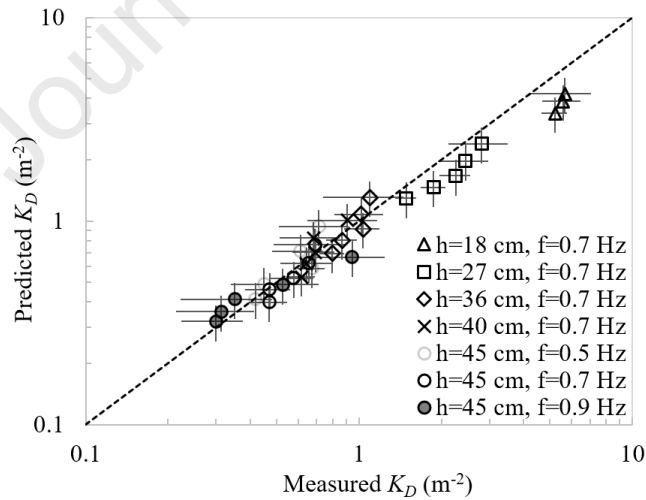


**Fig. 6** Comparison of predicted and measured wave decay coefficient  $K_D$ . The uncertainty in the measured  $K_D$  reflects the 95% confidence in fitted  $K_D$  from Eq. 6. The uncertainty in model prediction was 20%, based on the estimated uncertainty in the plant drag considering the uncertainties in  $C_D$ ,  $U_w$ ,  $C_s$ , the plant geometrical and mechanic properties (Zhang and Nepf, 2021).

## 4.2 Validation of model with measured wave decay in a live plant meadow

The model was used to predict the measured wave evolution over a live *Spartina anglica* meadow (Fig. 7) reported in Maza et al. (2015), Lara et al. (2016), and Losada et al. (2016). Five cases for wave condition R1 ( $a_w=0.075$  m,  $T_w=2$  s, see Table 1 in Maza et al., 2015) were extracted from Figure 3 and Figure 15 in Maza et al. (2015). The plant properties were listed in Tables 2 and 3 in Losada et al. (2016), which were the most detailed plant properties the authors could find in exist studies of wave dissipation by marsh plants. Their experimental data enabled the validation of the present model in representing the influence of both the geometric and mechanical properties of the leaves and the stem. Specifically, the plant had a 28.4-cm long stem and 5 leaves which were 17.8-cm long and 0.6-cm wide. The elastic modulus was 164.2 MPa and 77.6 MPa for the stem and the leaves, respectively. The stem diameter and leaf thickness were not reported. The stem diameter was assumed to be  $D=6$  mm, which was the same as the reported leaf width, and within the range of other reported values for *Spartina anglica* (Table 1). For the leaf thickness, a mean value  $d=0.46$  mm for *Spartina anglica* was reported in Li et al. (2009). The step size  $dx=0.2$  m was used in the model. Due to the finite width of the vegetation patch, wave diffraction was likely present, which is not considered in the present model. However, the model still captured the main mechanism of wave dissipation due to vegetation. The relative error between the measured and predicted amplitude,  $a_{w,x}/a_{w,0}$ , was  $14\% \pm 13\%$  (based on a total of 33 measuring points). The model tended to work better for deeper water depths and less well for the shallowest water depth ( $h = 0.4$  m, black and red curves in Fig. 7). This might be explained by greater nonlinearity for shallower water depth, which tended to add uncertainty in the model prediction. This comparison extended the validation of the model to a wider parameter space, covering  $0.4 \leq Ca_s \leq 1.6$ ,  $2.6 \leq L_s \leq 5.5$ ,  $239 \leq Ca_l \leq 1074$ ,  $1.6 \leq L_l \leq 3.4$ .

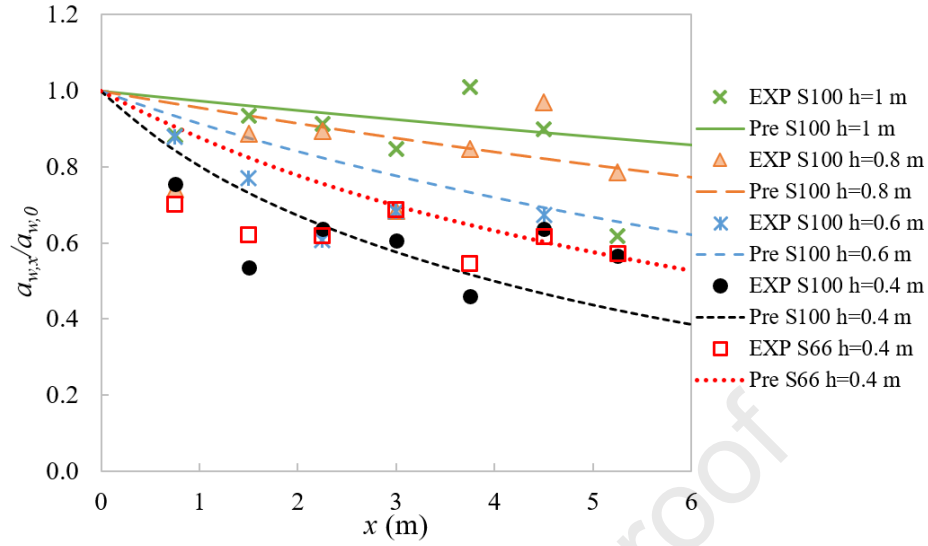


**Fig. 7.** The measured (symbols) and predicted (curves) wave amplitude,  $a_{w,x}$ , normalized by the upstream amplitude,  $a_{w,0}$ , as a function of distance across a circular patch of *Spartina anglica*. The measured data were extracted from Figure 3 and Figure 15 in Maza et al. (2015). S100 and S66 represent the density of *Spartina anglica* meadow, which are 729 and 430 plants/m<sup>2</sup>, respectively. The wave period was 2 s.

### 4.3 Validation of model with wave decay measured in the field

The model was further validated by wave attenuation measurements made by Garzon et al. (2019) in a *Spartina alterniflora* marsh in the Chesapeake Bay, USA, under storm surge conditions. The wave conditions were reported with pressure data measured at 4Hz at stations S1, S2, S3, and S4 (see Figure 1 in Garzon et al., 2019). The pressure data recorded from 2015.09.24 to 2015.09.30 was downloaded from Lab, M. F. H. R. (2019) and processed following Garzon et al. (2019) to obtain the water depth,  $h$ , and significant wave height,  $H_{m0}$  for each 10-min burst record. The average wave period for each 10-min record was obtained using the zero-crossing method (Zhang et al., 2020). In this section, the measured water depth, wave amplitude and wave period at S2 and S3 are used to validate our model. This 23-m long transect, labeled as S23, was chosen because the bottom is relatively flat compared to S12 (from S1 to S2) and S34 (from S3 to S4), see Figure 1d in Garzon et al. (2019), such that the effect of bottom on the wave dissipation was minimum. The measured water depth at S2 and S3 differed by less than 1 cm. The measured wave decay coefficient for transect S23 was determined using Eq. 13, i.e.,  $K_{D,Measured} = (2/H_{m0,S3} - 2/H_{m0,S2})/L_m$  and  $L_m = 23$  m is the length of the transect. At S23 the reported stem height

$l_s = 71 \pm 21$  cm, stem diameter  $D = 5 \pm 1.5$  mm, and stem density  $N_s = 344 \pm 80$  stems/m<sup>2</sup>. Based on sample plant images provide by Ferreira team, the plant is estimated to have 5 leaves per stem. A moderate leaf dimension ( $l_l = 30$  cm and  $b = 0.8$  cm) was chosen based on the reported stem parameters and the range of plant parameters for *Spartina alterniflora* listed in Table 1. The leaf thickness  $d = 0.34$  mm was the average leaf thickness for *Spartina alterniflora* reported by Maricle et al. (2009). The elastic modulus of leaf and stem was assumed to be  $E_s = E_l = 0.5$  GPa, with in the range of stem elastic modulus for *Spartina alterniflora* (Table 1). A 20% uncertainty in plant element rigidity ( $EI$ ) was considered in the model prediction to reflect a range of plant properties. The effect of plant rigidity will be discussed in more detail in section 4.5. Note that only data corresponding to  $h > 0.4$  was applied here for comparison. Further, the model described in section 2 assumed linear wave theory, such that the model only predicted the small nonlinearity wave conditions. Specifically, conditions correspond to a relative error for velocity predicted by linear wave theory and Stokes 2<sup>nd</sup> wave theory smaller than 20% (see Appendix B). The water depth and wave amplitude ( $a_w = 2/H_{m0,S2}$ ) at S2, and the mean wave period  $T_w = (T_{w,S2} + T_{w,S3})/2$  were used as the model input to predict the wave decay along the meadow. The predictions were made using  $dx = 0.5$  m and  $C_s = 0.6$ . For a total of 37 cases, the predicted  $K_D$  agreed with the measured wave decay coefficient to within  $9\% \pm 5\%$  relative error (Fig. 8). Note that the incoming wave direction at S2 was approximately  $30^\circ$  to the straight line between S2 and S3 (based on Figure 1c and the top sub plot of Figure 7 in Garzon et al., 2019), which was simplified to a 2-dimensional problem (wave direction assumed parallel to the line S2-S3), which added some uncertainty to the prediction. These comparisons extended the validation of the model to a wider parameter space (water depth, wave height, and wave period), covering  $2 \leq Ca_s \leq 11$ ,  $4.7 \leq L_s \leq 7.7$ ,  $682 \leq Ca_l \leq 1523$ ,  $2 \leq L_l \leq 3.8$ . Further, the comparison addressed the validity of the present model in capturing the wave dissipation by vegetation in the field conditions. The measured wave conditions, the measured and predicted wave decay coefficient, and the dimensionless parameters for these cases were summarized in Table S4 in the Supplementary Material.

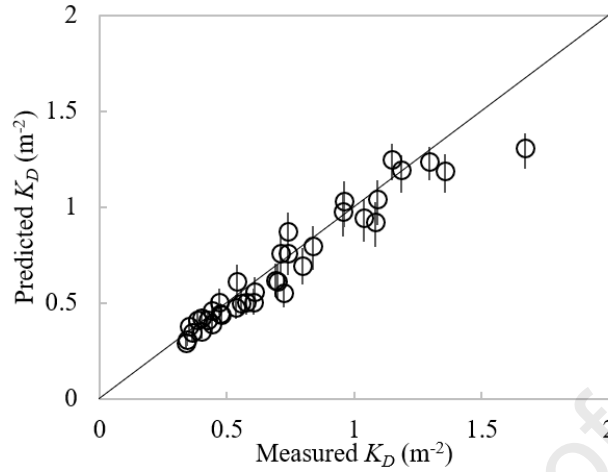


**Fig. 8.** Predicted  $K_D$  versus measured  $K_D$  for field transect S23 (Garzon et al., 2019). Model predictions were made over a 23-m long meadow with a plant density  $N_s = 344$  stems/m<sup>2</sup>, stem height  $h = 71$  cm, stem diameter  $D = 5$  mm, with 5 leaves per plant ( $l_l = 30$  cm,  $b = 0.8$  cm, and  $d = 0.34$  mm). The elastic modulus was assumed  $E_s = E_l = 0.5$  GPa for the stem and the leaves, respectively. The error bars indicate the difference considering a 20% error in the leaf ( $E_l I_l$ ) and stem rigidity ( $E_s I_s$ ).

#### 4.4 The impact of wave parameters on wave dissipation

The validated model was used to explore how wave parameters impact the wave decay associated with flexible marsh plants, using both the model plant (in the current study) and a live plant (*Spartina anglica* used in Maza et al., 2015; Lara et al., 2016; and Losada et al., 2016) under a wide range of water depth, wave amplitude, and wave period. Losada et al. (2016) reported a wave decay coefficient  $\beta$  (Table 4 in their paper) based on fitting the measured wave amplitudes along the meadow (7 measurements for each case) using  $\frac{a_{w,x}}{a_{w,0}} = \frac{1}{1+\beta x}$ . Comparing to Eq. 12, this was converted to the wave decay coefficient defined in the present study,  $K_D = \beta/a_{w,0}$ . The plant properties, meadow length, and shoot density were kept the same as the model plant (see Table 2 and description in section 2) and *Spartina anglica* (Tables 2 and 3 in Losada et al., 2016, the meadow length was 6 m and plant density was 729 plants/m<sup>2</sup>), respectively. The numerical experiments covered a wide range of Cauchy number and length ratio,  $0.01 \leq Ca_s \leq 1.7$ ,  $2.3 \leq L_s \leq 26$ ,  $1.8 \leq Ca_l \leq 1137$ , and  $1.3 \leq L_l \leq 16$  (Fig. 9). In general, the leaves actively reconfigured,  $Ca_l > 1$  and  $L > 1$ , while the stem varied from not moving ( $Ca_s < 1$ ) to moving ( $Ca_s > 1$ ). For both the model plants and the *Spartina anglica*, the wave decay coefficient  $K_D$  decreased with increasing water depth and increasing wave amplitude, but increased with

increasing wave period (Fig. 9). These trends generally agreed with measured values in the model plants in this study (circles in Fig. 9 a, b, and c) and values in the *Spartina anglica* meadow measured by Maza et al. (2015), Lara et al. (2016), and Losada et al. (2016) (circles Fig. 9 d, e, and f). Except for the  $T_w = 2.2$  s case (Fig. 9f), which exhibited unusually small measured wave damping, the relative error between the predicted and the measured  $K_D$  was  $33\% \pm 25\%$  (based on 7 independent cases). There was a greater uncertainty in predicting  $K_D$ , versus predicting wave amplitude along the meadow ( $14\% \pm 13\%$ , Fig. 7), because of the large variation in the amplitude measurements (see the symbols in Fig. 7). Nevertheless, considering the complexity of the problem and the large uncertainty in both the plant parameters and experiment measurements, the model prediction has done well. Next, we consider the dependencies on water depth, wave amplitude, and wave period.

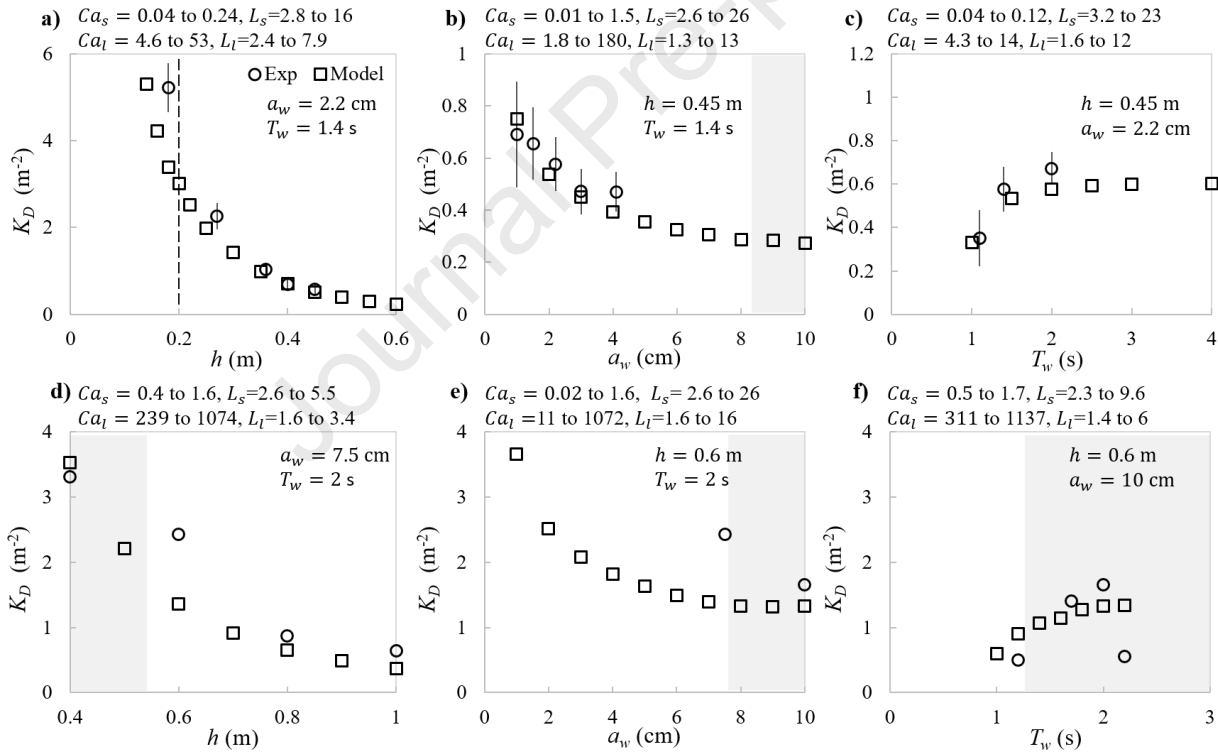


**Fig. 9.** Wave decay coefficient  $K_D$  over a 3.8 m model plant meadow (a, b and c) and over a 6 m *Spartina anglica* meadow (d, e, and f). The circles are measurements from the present study (first row) and from Losada et al. (2016) (bottom row). The squares are predictions made with  $C_s = 0.6$  and  $dx = 0.2$  m based on Eqs. 7 through 13. The range of Cauchy number and length ratio for the leaf and stem are listed above each subplot. The shaded area indicates  $Ca_s > 1$ . The vertical dashed line in subplot a) indicates the height of the plant stem.



First,  $K_D$  decreased rapidly with increasing water depth, which has also been observed in field measurements (Ysebaert et al., 2011; Yang et al., 2012; Zhang et al., 2020). As a reference point, consider a rigid plant ( $Ca < 1$ ), for which the force on the plant scales with the wave velocity and plant frontal area,  $F_r \sim U_w^2 A$ . Based on Eq. 11, when the wave amplitude and wave period are held constant,  $U_w$  decreases with increasing  $h$ . When the plant is emergent, the frontal area exposed to hydrodynamic drag scales with the water depth  $h$ , but, when the plant is submerged the front area scaled with the plant height  $h_p$ , which is a constant. As a result, in both regimes (emergent and submerged)  $F_r$  decreases with increasing  $h$ , but has a different scaling for emergent ( $F_r \sim U_w^2 h$ ) and submerged ( $F_r \sim U_w^2 h_p \sim U_w^2$ ) conditions. Specifically, for an emergent plant, the increase in water depth  $h$  offsets the decrease in  $U_w$ , such that the depth dependence of  $K_D$  is weaker for an emergent plant, compared to a submerged plant. This change in force scaling between emergent and submerged conditions produces an inflection point in  $K_D$  predicted by the theoretical expression developed by Dalrymple et al. (1984) for a meadow of rigid plants, see e.g., Figure. 8 in Zhang et al. (2020). However, the field values of  $K_D$  measured by Zhang et al. (2020) decrease smoothly with increasing  $h$ , i.e., did not exhibit an inflection point. Similarly, the model presented in this study predicts a smooth variation in  $K_D$  as a function of water depth (Fig. 9 a and d). This can be attributed to the plant flexibility. Specifically, when the plant reconfigures ( $Ca > 1$ ), and the plant length is greater than the wave orbital excursion ( $L > 1$ , as considered here), the plant drag is reduced (compared to rigid plant) by the plant motion. Previous studies have shown that the drag on a flexible plant ( $F_d$ ) decreases relative to drag on an identical rigid plant ( $F_r$ ) in proportion to  $(CaL)^{-1/4}$  (Luhar and Nepf, 2016; Lei and Nepf, 2019a), i.e.,

$$F_d \sim F_r (CaL)^{-1/4} \sim U_w^2 h_p (U_w h_p^4)^{-1/4} \sim U_w^{7/4} \quad (14)$$

The right-most expression was obtained by using the definitions of  $Ca$  (Eq. 2) and  $L$  (Eq. 3), with the submerged plant length  $h_p$  replacing  $l$ , and isolating the parameters  $h_p$  and  $U_w$ . Note that the plant height cancels in the expression (Eq. 14), indicating that in the regime  $Ca > 1$  and  $L > 1$  the length of a flexible plant does not impact the plant drag, which explains why  $K_D$  decreased smoothly (without an inflection point) with increasing  $h$  (Fig. 9a and d).

Second,  $K_D$  decreased with increasing wave amplitude  $a_w$  (Fig. 9b and e). A reduction in wave decay with increased wave amplitude has also been observed in live *Puccinellia maritima*



and *Spartina anglica* meadows (see R1 and R2 in Figure. 6 in Maza et al., 2015). For rigid plants ( $Ca < 1$ ), the Dalrymple et al. (1984) model indicates that  $K_D$  is influenced by  $a_w$  only through the drag coefficient, i.e.,  $K_D \sim C_D$ . Specifically, the drag coefficients for rigid leaves and stems dependent on the Keulegan-Carpenter number (Fig. A.1 in Appendix A), which is proportional to wave amplitude, i.e.,  $KC = U_w T_w / D \sim a_w$ . For the range of predictions made here,  $KC_l > 10$  and  $KC_s > 25$ , which corresponded to  $C_{D,l} \sim KC_l^{-1/3} \sim a_w^{-1/3}$  and  $C_{D,s} \sim KC_s^{-0.2} \sim a_w^{-0.2}$ , which implied  $K_D \sim a_w^{-0.33 \text{ to } -0.2}$ . For flexible plants ( $Ca > 1$ ), an additional dependence comes from the reconfiguration scaling,  $F_d \sim F_r (CaL)^{-1/4}$  (e.g., Zhang and Nepf, 2021). The wave force due to plant reconfiguration makes the plant more streamlined and also reduces the relative motion between the wave and the plant. Both mechanisms decrease the force on the plant, and thus decrease the wave dissipation. The wave decay coefficient  $K_D$  has a unit [ $m^{-2}$ ], which is the relative wave dissipation per meadow length per wave amplitude (Eq. 12). Combining with the wave energy dissipation per meadow length  $E_D$  ( $\sim F_d U_w$ , Eq.9),  $K_D \sim (E_D / E_w) a_w^{-1}$ , in which  $E_w \sim a_w^2$  is the wave energy. After some algebra  $K_D \sim F_d / U_w^2 \sim (CaL)^{-1/4} \sim U_w^{-1/4} \sim a_w^{-1/4}$ . Combining this with the drag coefficient dependence, we expect  $K_D \sim C_D (CaL)^{-1/4} \sim a_w^{-0.58 \text{ to } -0.45}$ , with the lower value exponent corresponding to the drag contributed from the leaves and the higher value from the stem. Consistent with this, the model predicted  $K_D = (0.089 \pm 0.003) a_w^{-0.46 \pm 0.01}$  for the model plants (Fig. 9b) and  $K_D = (0.40 \pm 0.04) a_w^{-0.48 \pm 0.03}$  for *Spartina anglica* (Fig. 9e). This agreement in amplitude dependence demonstrated that the model correctly captured the impact of plant reconfiguration for both the model and live plants.

Third,  $K_D$  increased rapidly with increasing wave period for small wave period,  $1 \leq T_w \leq 2$  s, but increased only slightly for  $T_w > 2$  s (Fig. 9c and f). As  $T_w$  increased from 1 to 2 s,  $kh$  decreased from 1.9 to 0.3 (Fig. 9c) and 2.5 to 0.9 (Fig. 9f), indicating a shift towards shallower water waves, which is associated with a velocity distribution that is increasingly more uniform. At the same time, since the water depth and wave amplitude were held constant,  $U_w$  increased with the increasing  $T_w$  until it approached a constant value (Eq. 11). The hydrodynamic force for a rigid plant (as a baseline condition),  $F_d \sim U_w^2$ , and the wave energy dissipation follows these trends,  $E_D \sim U_w^3$  (Eq 9), so that  $K_D$  had the same trends with increasing  $T_w$ , initially increasing but then reaching

a constant value. Further, for flexible plants,  $F_d/F_r \sim (CaL)^{-\frac{1}{4}} \sim U_w^{-\frac{1}{4}} T_w^{\frac{1}{4}}$ . Finally, the wave period also affect the plant force and energy dissipation by adjusting the drag coefficient, which scales as  $C_{D,l} \sim KC_l^{-1/3} \sim T_w^{-1/3}$  and  $C_{D,s} \sim KC_s^{-0.2} \sim T_w^{-0.2}$ . In combination,  $F_d \sim U_w^{\frac{7}{4}} T_w^{-\frac{1}{12} \text{ to } \frac{1}{20}}$ ,  $K_D$  increased with increasing  $T_w$  for small wave period but approached a constant value at large wave period mainly due to the modification of  $T_w$  on  $U_w$ . Losada et al. (2016) also observed a rapid increase in wave decay in live *Spartina anglica* meadows when wave period increased from 1.2 to 2 s (see circles in Fig. 9 f above and Table 4 in their paper), which agreed with the model prediction.

#### 4.5 The impact of plant properties on wave dissipation

Previous studies have shown a positive correlation between plant biomass and wave dissipation for both live plants (e.g., Maza et al., 2015; Rupprecht, 2015) and mimic model plants (Paul et al., 2012). More recently, simulations comparing the biomass and frontal area of several marsh species showed that the frontal area per bed area was a better predictor of wave drag per bed area, suggesting it would be a better predictor of wave dissipation (Figure 14 in Zhang and Nepf, 2021). To further deepen our understanding of how plant geometry and rigidity impact the wave dissipation, this section explores the impact of plant properties on the wave decay coefficient,  $K_D$ , including variation in stem and leaf geometry and mechanical properties. The predictions were made for the same wave condition ( $h = 1$  m,  $a_w = 10$  cm, and  $T_w = 2$  s) over a 3.8 long meadow with a plant density of 280 plants/m<sup>2</sup>. The following range of plant parameters were considered:  $l_s = 0.2$  to 1 m,  $D = 0.3$  to 2 cm,  $E_s = 0.03$  to 16 GPa,  $l_l = 0.1$  to 0.5 m,  $b = 0.4$  to 2 cm,  $d = 0.48$  mm, and  $E_l = 0.4$  to 33 GPa. These parameters covered a wide range of marsh plant properties in the field (Table 1), corresponding to the dimensionless parameter ranges  $0.05 \leq Ca_s \leq 40$ ,  $3 \leq L_s \leq 12$ ,  $2 \leq Ca_l \leq 421$ , and  $1.4 \leq L_l \leq 6$  (Fig. 10). In general,  $K_D$  increased with stem diameter  $D$ , leaf width  $b$ , stem rigidity  $E_s l_s$  and leaf rigidity  $E_l l_l$  (Fig. 10), while the stem length  $l_s$  and leaf length  $l_l$  had a smaller influence on  $K_D$ .

First, consider the stem and leaf lengths. Increasing  $l_s$  and  $l_l$  were both associated with greater frontal area per plant, which would tend to increase  $K_D$ . However, this trend was only observed when the plants did not reconfigure ( $Ca < 1$ ). Specifically, for shorter stems ( $l_s \leq 0.5$  m),  $Ca_s < 1$  (white region in Fig. 10a), and for this range  $K_D$  increased linearly with increasing  $l_s$ . In contrast,

when the stems reconfigured ( $Ca_s > 1$ , grey region in Fig. 10a), increasing  $l_s$  tended to decrease  $K_D$ . This is because the stem motion increased with increasing Cauchy number,  $Ca \sim l^3$ , which reduced both the leaf and stem associated plant force. In contrast, the leaves reconfigured ( $Ca_l > 1$ ) over the entire parameter range, and  $K_D$  had no obvious dependence on  $l_l$  (Fig. 10d). This was consistent with the reconfiguration scaling shown in Eq.14, which indicates that, in the flexible regime  $Ca > 1$  and  $L > 1$ , the drag on a plant element is not a function of the element length.

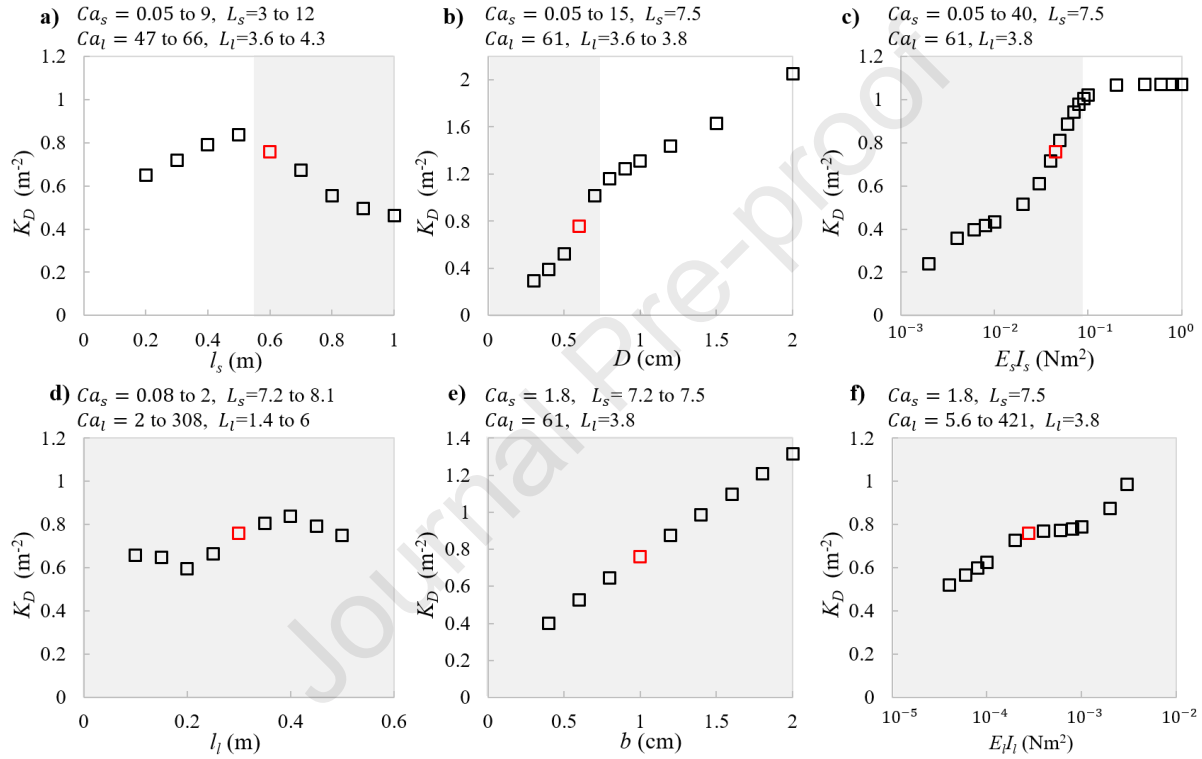


**Fig. 10.** Wave decay coefficient  $K_D$  predicted from Eqs. 7 through 13 versus a) the stem length  $l_s$ , b) stem diameter  $D$ , c) stem rigidity  $E_s I_s$  ( $D = 0.6$  cm), d) leaf length  $l_l$ , e) leaf width  $b$ , and f) leaf rigidity  $E_l I_l$  ( $b = 1$  cm and  $d = 0.48$  mm) predicted with  $dx = 0.2$  m,  $C_s = 0.6$ ,  $h = 1$  m,  $a_w = 10$  cm,  $T_w = 2$  s,  $N_s = 280$  stems/m<sup>2</sup>, and  $N_l = 10$  leaves/plant. The red squares shown in each subplot are an identical case included as a reference in each of the subplots and which corresponded to  $l_s = 0.6$  m,  $D = 0.6$  cm,  $l_l = 0.3$  m,  $b = 1$  cm,  $d = 0.48$  mm,  $E_l = 3$  GPa, and  $E_s = 0.7$  GPa. The range of leaf ( $Ca_l$ ) and stem ( $Ca_s$ ) Cauchy number, and length ratio,  $L$ , are listed above each subplot. The shaded area indicates  $Ca_s > 1$ .

Second, consider the plant dimensions in the transverse direction, i.e., the stem diameter and the leaf width. When the stem did not reconfigure ( $Ca_s < 1$ ),  $K_D$  increased approximately linearly with  $D$  (white region,  $D > 7$  mm, in Fig. 10b). This was consistent with frontal area increasing

linearly with  $D$ . When the stem was able to reconfigure ( $Ca_s > 1$ , grey area,  $D \leq 7$  mm, in Fig. 10b),  $K_D$  increased with increasing  $D$ , but the dependence was non-linear, with  $K_D$  increasing with  $D$  to power greater than 1. The non-linear dependence on stem diameter for flexible conditions was due to the influence of stem rigidity  $E_s I_s \sim D^4$ , which influenced the Cauchy number  $Ca_s \sim D^{-3}$ . Specifically, increasing  $D$  was associated with decreasing Cauchy number, which, in turn, decreased the motion of the flexible stem. As stem motion decreased, the stem drag and wave dissipation increased. Further, the stem diameter also affected the plant drag through the drag coefficient ( $C_{D,s} \sim KC_s^{-0.2} \sim D^{0.2}$  for  $23 \leq KC_s \leq 150$ ). Combining these dependencies,  $F_d \sim C_D D \sim D^{1.2}$  and  $F_d \sim C_D D (Ca_s L_s)^{-1/4} \sim D^{1.95}$  for rigid stem ( $Ca_s < 1$ ) and flexible stem ( $Ca_s > 1$ ), respectively. These scales explained the observation in Fig. 10b that plant drag and thus wave dissipation increased with increasing  $D$ , but increased faster with  $D$  for flexible conditions ( $Ca_s > 1$ ). In contrast, the leaf rigidity (and thus leaf Cauchy number  $Ca_l$ ), is not a function of leaf width,  $b$ , such that the leaf width  $b$  only affected the leaf frontal area, and  $K_D$  had an approximately linear dependence on  $b$  over the full parameter range (Fig. 10e).

Third, consider the stem and leaf rigidity,  $EI$  (Fig. 10c and f). In the parameter range for which the stem and leaves can reconfigure (grey shading indicates  $Ca_s > 1$  in Fig. 10c and f), the degree of reconfiguration decreased as  $E$  increased, resulting in higher values of  $K_D$ . By comparison,  $E_s$  had a weaker influence on  $K_D$  than did  $D$  (Fig. 10b and c), because rigidity  $E_s I_s$  is proportional to  $D^4$ , but only linearly proportional to  $E_s$ . For conditions with  $Ca_s < 1$  (white region in Fig. 10c), the stem did not reconfigure, and  $K_D$  was a constant, i.e., had no dependence on  $EI$  (Fig. 10c). A similar trend has been observed in the laboratory measurements of wave damping by cylinders of varied flexural rigidity (Paul et al., 2012; Tan et al., 2019; van Veelen et al., 2020). For example,  $K_D$  for minimum stem rigidity tested  $E_s I_s = 0.002 \text{ Nm}^2$  ( $Ca_s = 40$ ) was 78% smaller than that of the rigid limit (Fig. 10c), which was comparable to the experimental results of van Veelen et al., (2020), in which flexible cylinders attenuate waves as much as 70% less than rigid cylinders. For the wave conditions tested here, the leaves reconfigured ( $Ca_l < 1$ ) even for  $E_l I_l = 0.003$ , which correspond to the upper limit for marsh plant leaf rigidity in the field (e.g.,  $b = 1$  cm,  $d = 0.48$  mm and  $E_l = 33$  GPa). That is, the reconfiguration of leaves is always important at the field scale.

Next, the leaf associated force increased nearly linearly with leaf number  $N_l$ , and this

translated to a similar dependence for  $K_D$  (Fig. 11). For plants without leaves,  $K_D = 0.21 \text{ m}^{-2}$ , which was only 27% of the  $K_D$  for a plant with 10 leaves (red square in Figs. 9 and 10). Note that, with the increase in leaf number, the distributed force on the stem due to the leaves also increased ( $f_l$  in Eq. 7), enhanced the stem motion, which in turn, reduced the plant force. That is why the predicted  $K_D$  increased less than linearly with  $N_l$  (larger  $K_D$  fall below the dash line in Fig. 11).

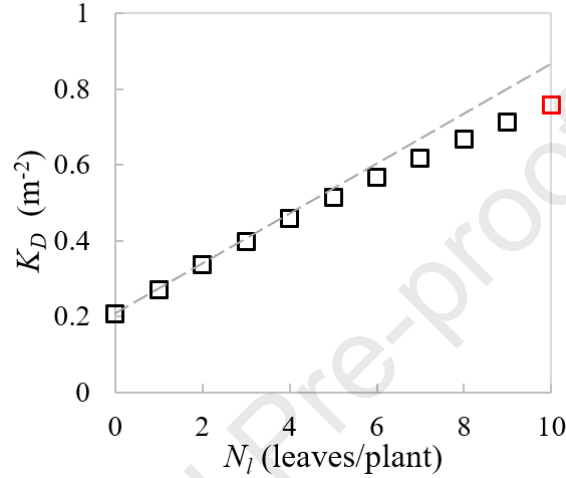


**Fig. 11.** Impact of leaf number on wave decay coefficient  $K_D$ . The predictions were made with  $dx = 0.2 \text{ m}$ ,  $C_s = 0.6$ ,  $h = 1 \text{ m}$ ,  $a_w = 10 \text{ cm}$ ,  $T_w = 2 \text{ s}$ ,  $N_s = 280 \text{ stems/m}^2$ ,  $l_s = 0.6 \text{ m}$ ,  $D = 0.6 \text{ cm}$ ,  $l_l = 0.3 \text{ m}$ ,  $b = 1 \text{ cm}$ ,  $d = 0.48 \text{ mm}$ ,  $E_l = 3 \text{ GPa}$ , and  $E_s = 0.7 \text{ GPa}$ . The red square shows the same case labeled red in Fig. 10. The dashed line indicates a linear trend.

Finally, this study examined four plant densities,  $280 \text{ stems/m}^2$  (the model plants, section 4.1),  $344 \text{ stems/m}^2$  (the *Spartina alterniflora* in the field, section 4.3),  $430$  and  $729 \text{ stems/m}^2$  (the live *Spartina anglica* plants in the laboratory experiment, section 4.2). For each of these densities, our model provided good prediction of measured decay, suggesting that the assumption of negligible plant interaction may be appropriate for this range of plant area density (or solid volume fraction  $A_c N_s$ ). For meadows of higher area density, plant interaction may be present in three forms. First, when the plant spacing is small compared to the wave excursion, the wave velocity within the canopy may be diminished (Lowe et al., 2005). This type of plant interaction can be accounted for by using the in-canopy volume averaged flow velocity in the prediction of the wave dissipation. This has been described in Hu et al. (2014), Lei and Nepf (2019a), and van Veelen et al. (2021). For example, using the in-canopy velocity, van Veelen (2021) predicted the wave damping by a meadow of dense cylinders ( $1111 \text{ stems/m}^2$ ). Second, for a dense emergent meadow, the wave

velocity can be enhanced around individual stems due to the constricted cross-sections (termed “blockage effect” in Etminan et al., 2019). This blockage effect has been shown to increase the canopy drag coefficient for meadows with a solid fraction  $\geq 0.06$  (Etminan et al., 2019). However, in marshes the solid volume fraction is generally much smaller than 0.06, partly because the densest meadows are usually associated with a relatively smaller stem diameter (e.g., see Table 1 and the references listed). Even considering the maximum stem diameter and maximum plant density for the *Spartina alterniflora* and *Spartina anglica* listed in Table 1, the solid volume fraction is still less than 0.045, suggesting that the blockage effect might not be important for marsh plant meadows. Third, in conditions with large reconfiguration, the direct contact between plants may restrict the plant motion. This contact will mostly occur between leaves. Since the leaf tips are following the wave motion, they contribute little to the total plant force, so that any changes in total plant force associated with leaves contacting neighboring plants will be small. At the same time, the lower part of the plant, which contributes the most of the plant drag, normally cannot deflect enough to touch a neighboring plant. Further, all the plants are moving in a similar way, such that, even if contact occurs, the relative velocity will be small. This description is supported by two previous studies, videos of flexible plant motion in a meadow can be found in the study of Lei and Nepf (2019a) (<https://news.mit.edu/2019/study-seagrass-erosion-0503>) and the supplementary material in van Veelen et al. (2020). Based on the above discussion, we cautiously suggest that contact between plants should not significantly impact plant drag, and that the neglect of plant contact is reasonable. However, this conclusion should be validated in future studies.

## 5 Conclusion

This paper dynamically modeled the motion of and force on an individual marsh plant and used the modeled force to predict the wave damping across a marsh meadow. The prediction of wave energy dissipation agreed with experimental measurements over a meadow of model plants, a patch of live *Spartina anglica* (Losada et al., 2016), and also within a *Spartina alterniflora* marsh in the field (Garzon et al., 2019). These validations covered a wide range of dimensionless parameters in the field (Table 1). Specifically,  $0.01 \leq Ca_s \leq 11$ ,  $2.6 \leq L_s \leq 44$ ,  $0.9 \leq Ca_l \leq 1523$ ,  $1.6 \leq L_l \leq 22$ . The validations showed that the linear wave theory based wave damping model can be applied to weakly nonlinear wave conditions. A systematic set of simulations showed

that for a given marsh,  $K_D$  depends most strongly on the water depth. Specifically,  $K_D$  decreased with increasing water depth.  $K_D$  also decreased with increasing wave amplitude, which reflected increasing plant reconfiguration.  $K_D$  increased with increasing wave period up to 2 s, and then became insensitive to further increases in period, and this was attributed to changes in wave velocity. Under the same wave conditions,  $K_D$  increased with stem height, stem diameter, leaf width, and the rigidity of the stem and the leaf, as well as the number of leaves on a stem. Importantly, while leaves contributed significantly to plant drag and thus wave dissipation, in the regime  $Ca > 1$  and  $L > 1$ , which is typical of field conditions, the drag on the leaf was not a function of the leaf length, such that leaf length had negligible influence on  $K_D$ . This study highlighted the importance of plant morphology and material properties on wave dissipation. Based on this, in order to achieve better prediction of coastal protection, the characterization of marsh wave dissipation must reflect plant morphology and rigidity.

#### Acknowledgment

We thank Dr. Jiarui Lei for his guidance with the experimental equipment. Xiaoxia Zhang was supported by the China Scholarship Council. The project also received support from the US National Science Foundation under EAR 1659923. Any opinions, findings, and conclusions in this paper are those of authors and do not necessarily reflect the views of the China Scholarship Council or the US National Science Foundation.

#### Appendix A. Drag and inertia coefficients

The drag coefficient  $C_D$  and the inertial coefficient  $C_M$  for the leaf (represented by a flat plate) and stem (represented by a circular cylinder) both depend on the Keulegan and Carpenter number, defined as  $KC_s = U_w T_w / D$  for the stem and  $KC_l = U_w T_w / b$  for the leaf. Expressions for  $C_D$  and  $C_M$  were fitted from the experimental data reported in Keulegan and Carpenter (1958) (Fig. A.1). These fitted coefficients were applied in the simulation of plant motion and drag. Due to the insufficient data for  $KC > 100$ , the  $C_M$  value for  $KC > 100$  was assumed constant and equal to  $C_M$  at  $KC = 100$ . The drag coefficient limit at large  $KC$  was set to the  $C_D$  for steady current. Specifically,  $C_{D,l} = 1.95$  and  $C_{D,s} = 1$  for the leaf and stem, respectively at large  $KC$ .



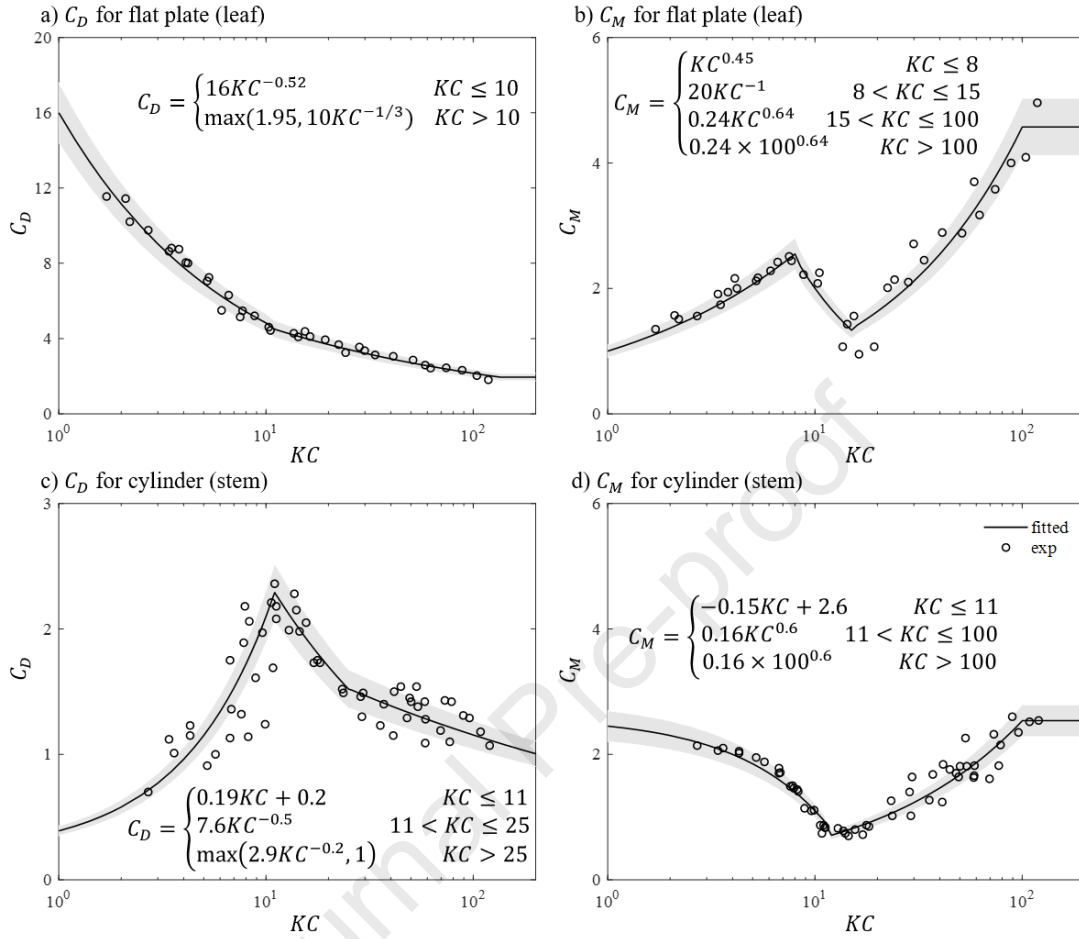


**Fig. A.1** The comparison of the fitted  $C_D$  and  $C_M$  for the leaf and stem versus the measured  $C_D$  and  $C_M$  for rigid plates and rigid cylinders by Keulegan and Carpenter (1958).

## Appendix B. Discussion of linear wave assumption

First, the meadow and wave conditions considered in our experiments corresponded to canopy independent flow, in which the impact of canopy drag on the linear wave motion within the canopy is negligible (Lowe et al., 2005). First, the solid volume fraction  $\lambda_p = 1.4 \times 10^{-4} \ll 1$ . Second, the space between two neighbor plants,  $S$ , was much larger than the stem diameter ( $S/D=30 \gg 1$ ) and smaller than the wave orbital excursion ( $0.07 \leq A_w/S \leq 0.9$ ). Both indicate small in-canopy velocity reduction based on Lowe et al. (2005).

Second, wave velocity profiles measured at the leading and trailing edge (Fig. B.1) generally conformed to linear wave theory. Specifically, the measured wave velocity closely matched the maximum horizontal velocity predicted by the linear wave theory (Fig. B.1). Note that



measurements near  $z=10, 20$ , and  $30$  cm were excluded, as these correspond to the weak spot of the Vectrino with low signal to noise ratio. To simplify the modeling, the depth-averaged orbital velocity  $\tilde{u}$  (Eq. 11) was used in the simulation. Compared to the vertically-varied velocity, using a depth-average velocity contributed less than 2% deviation in the force on the plant ( $= \left| (1/h_p) \int_0^{h_p} u_w^2(z) dz - \tilde{u}^2 \right| / \tilde{u}^2$ ) and less than 4% deviation in the wave energy dissipation ( $= \left| (1/h_p) \int_0^{h_p} u_w^3(z) dz - \tilde{u}^3 \right| / \tilde{u}^3$ ). The velocity profiles for all tested conditions were summarized in Table S2 in the Supplementary Material.

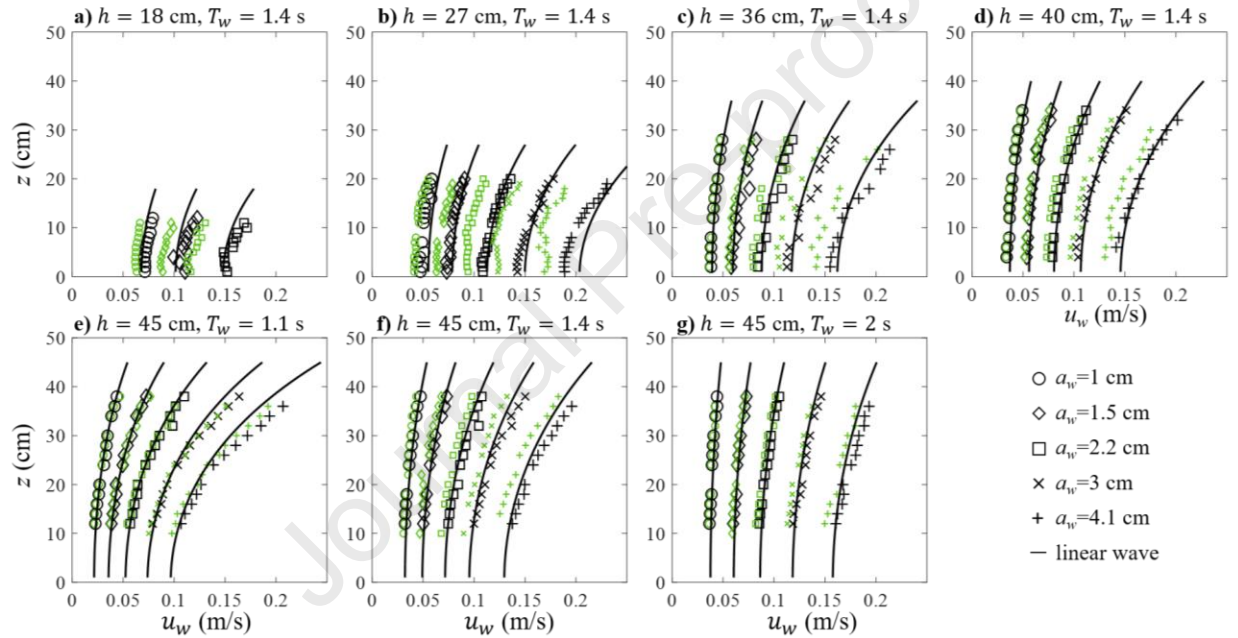


**Fig. B.1** The measured velocity profiles at the leading edge (black symbols) and at the trailing edge of the meadow (green symbols). The solid curves are predicted linear wave velocity at the leading edge of the meadow.

We note that the phase-averaged wave velocity in the experiment deviated slightly from linear wave theory, but the impact of this deviation was small (less than 10%). For example, Fig. B.2 compares the measured phase-averaged velocity (circles) to linear wave theory (solid curve) and first order non-linear wave theory, i.e., Stokes 2<sup>nd</sup> wave (dashed curve) for  $h = 40$  cm,  $T_w = 1.4$  s, and  $a_w = 4.1$  cm. The relative error between the measured and predicted velocity ( $=$

670  $\frac{1}{2\pi} \int_0^{2\pi} (u_{exp}(\phi) - u_{pre}(\phi)) d\phi / U_w$  ), plant force (  $= \int_0^{2\pi} u_{exp}(\phi)^2 - u_{pre}(\phi)^2 d\phi /$   
 671  $\int_0^{2\pi} u_{exp}(\phi)^2 d\phi$  ), and energy dissipation (  $\int_0^{2\pi} u_{exp}(\phi)^2 |u_{exp}(\phi)| - u_{pre}(\phi)^2 |u_{pre}(\phi)| d\phi /$   
 672  $\int_0^{2\pi} u_{exp}(\phi)^2 |u_{exp}(\phi)| d\phi$  ) were 11%, 0.6%, and 0.2% for linear wave theory, and 11%, 1%, and  
 673 0.6% for Stokes 2<sup>nd</sup> order wave theory, respectively. Sub-scripts ‘exp’ and ‘pre’ denoted the  
 674 experimentally measured and theoretically predicted velocity, respectively.

675 Due to the non-linearity in the experimental wave conditions (Fig. B.2), the model predictions  
 676 based on linear wave theory could underestimate wave dissipation. However, this effect was  
 677 estimated to be small. This was concluded by comparison between linear wave theory (Eq. 11) and  
 678 Stokes 2<sup>nd</sup> order wave theory (denoted by subscripts ‘linear’ and ‘S2’, respectively), as almost all  
 679 wave conditions are weakly nonlinear and are within or near the range of Stokes 2<sup>nd</sup> wave condition  
 680 (Fig. B.3). The relative error between the wave orbital velocity (  $= \frac{1}{2\pi} \int_0^{2\pi} u_{S2}(\phi) -$   
 681  $u_{linear}(\phi) d\phi / U_w$  ), plant force (  $= \frac{1}{2\pi} \int_0^{2\pi} |u_{S2}(\phi)| u_{S2}(\phi) - |u_{linear}(\phi)| u_{linear}(\phi) d\phi /$   
 682  $\frac{1}{2\pi} \int_0^{2\pi} |u_{linear}(\phi)| u_{linear}(\phi) d\phi$  ), and energy dissipation (  $= \frac{1}{2\pi} \int_0^{2\pi} |u_{S2}(\phi)| u_{S2}(\phi)^2 -$   
 683  $|u_{linear}(\phi)| u_{linear}(\phi)^2 d\phi / \frac{1}{2\pi} \int_0^{2\pi} |u_{linear}(\phi)| u_{linear}(\phi)^2 d\phi$  ) were  $7\% \pm 5\%$  (23%),  $2\% \pm$   
 684  $2\%$  (14%), and  $4\% \pm 5\%$  (29%) on average  $\pm$  SD (maximum) for all wave conditions in this study  
 685 (a total of 127 wave conditions covered in section 4). These small differences were considered  
 686 reasonable, such that wave non-linearity could be neglected for the experiments reported in this  
 687 study.

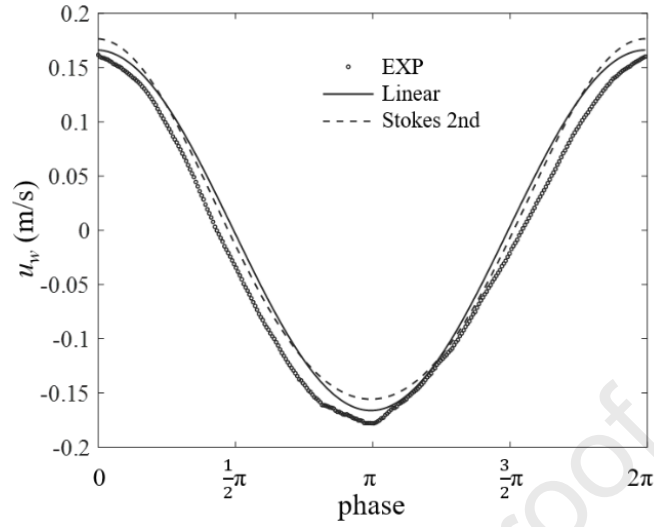


**Fig. B.2** Comparison of measured and predicted depth-averaged horizontal velocity over the stem height for test conditions  $h = 40$  cm,  $T_w = 1.4$  s, and  $a_w = 4.1$  cm.

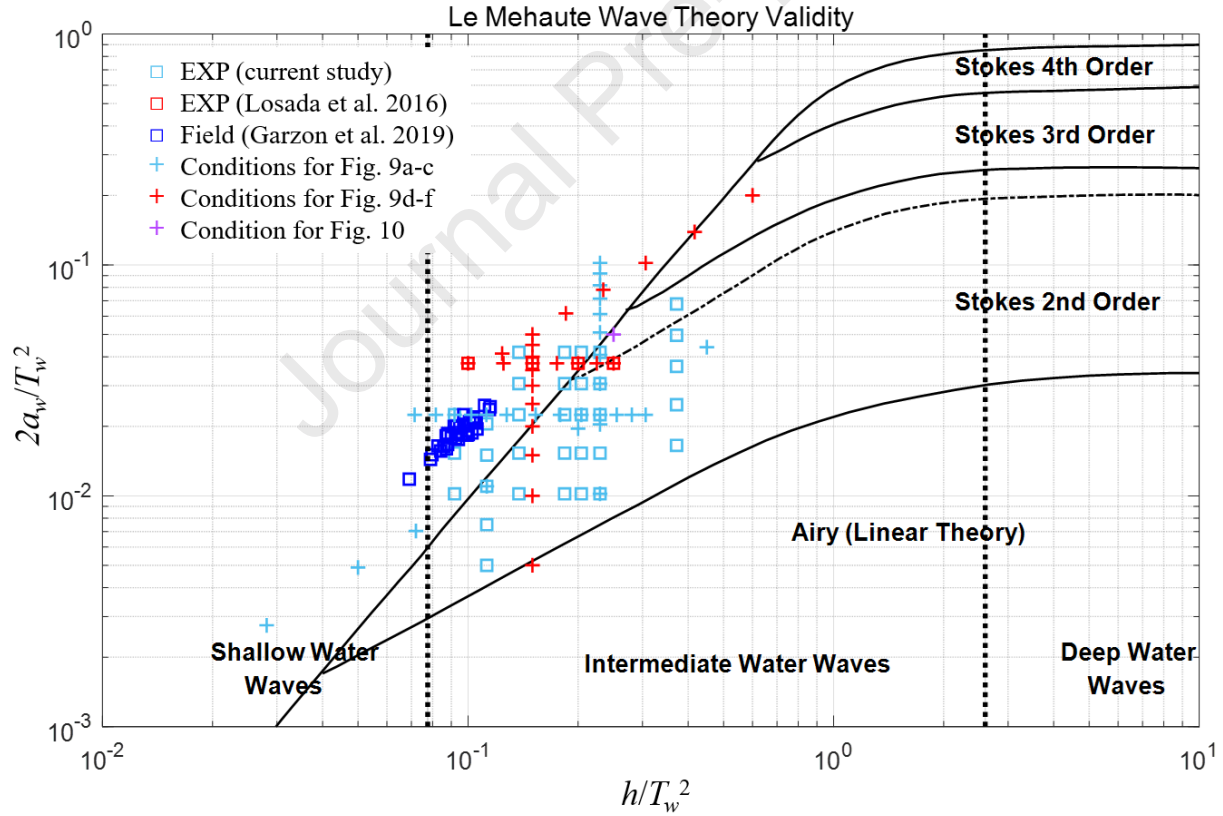


**Fig. B.3** The validity of wave theories for the wave conditions used in the current study. Squares and plus symbols represent the validation and application conditions, respectively.

### Appendix C. wave amplitude along the flume $a_{w,x}$

The wave amplitude measured over the meadow is shown in Fig. C.1 (black symbols). For  $h = 18, 27$ , and  $40$  cm, wave decay in the channel without plants was measured at three wave amplitudes. The wave decay coefficient estimated for the bare channel (baseboards and the flume wall) using Eq. 6, is reported in Fig. C.2, with subscript ‘b’ denoting bare channel.  $K_{D,b}$  followed a fitted relation  $K_{D,b}\lambda a_w = (0.18 \pm 0.1)e^{-(4.5 \pm 2)h}$ . To obtain the wave decay coefficient attributed to the plants alone ( $K_D$ ), the bare channel wave decay coefficient,  $K_{D,b}$  was subtracted from the total wave decay coefficient  $K_{D,T}$  measured with plants. The wave amplitude for all tests with and without plants was summarized in Table S1 in the Supplementary Material.

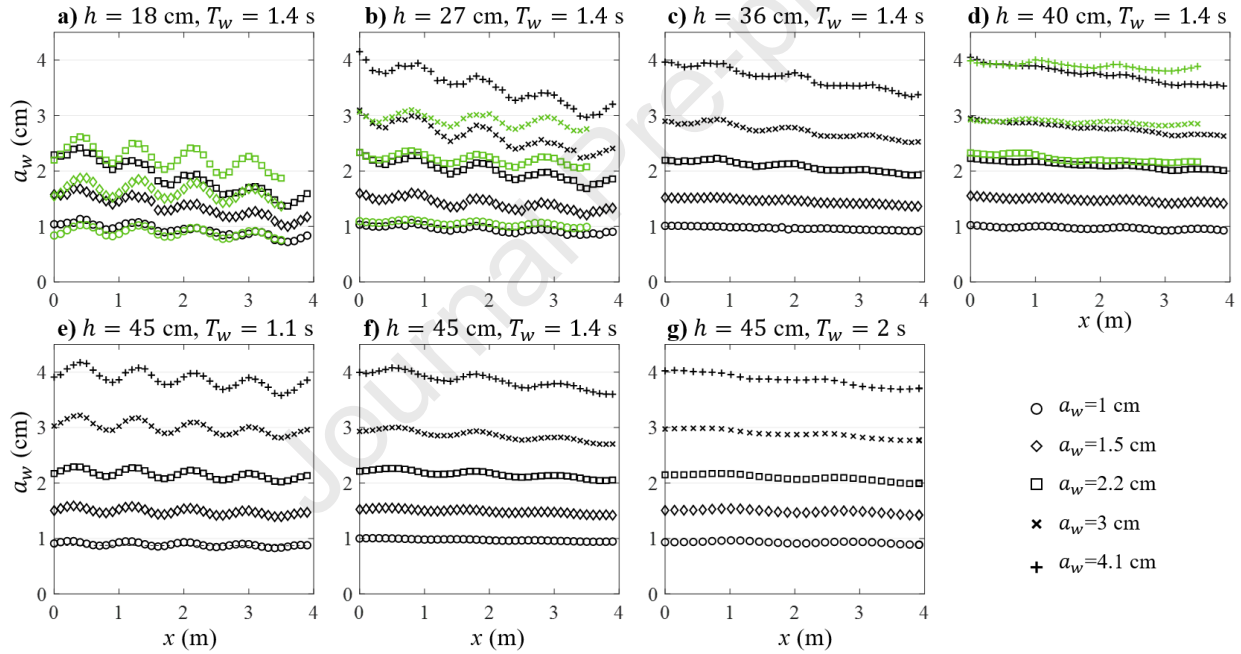


**Fig. C.1** Measured wave decay over the flume within the meadow (black symbols) and over the channel without plants (green symbols).

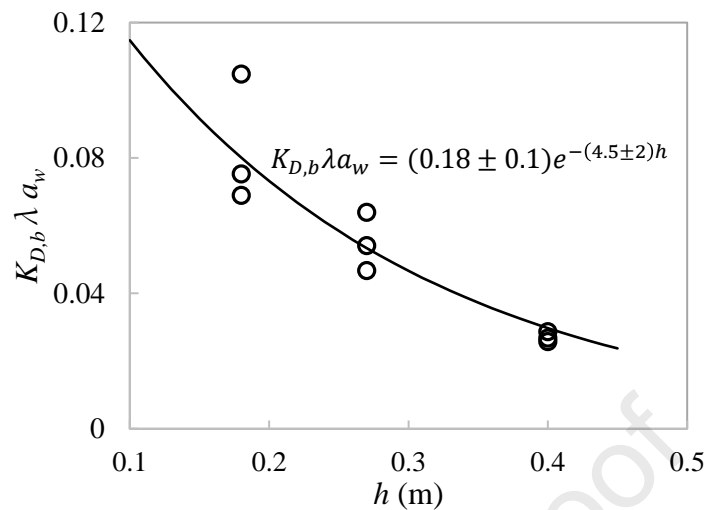


**Fig. C.2** Dimensionless wave decay over the channel without plants (circles). The black curve indicates the fitted relation between wave decay and water depth.

## References

- Anderson, M.E., Smith, J.M., 2014. Wave attenuation by flexible, idealized salt marsh vegetation. *Coastal Engineering* 83, 82–92. <https://doi.org/10.1016/j.coastaleng.2013.10.004>
- Arkema, K.K., Griffin, R., Maldonado, S., Silver, J., Suckale, J., Guerrey, A.D., 2017. Linking social, ecological, and physical science to advance natural and nature-based protection for coastal communities. *Ann. N.Y. Acad. Sci.* 1399, 5–26. <https://doi.org/10.1111/nyas.13322>
- Barbier, E.B., Hacker, S.D., Kennedy, C., Koch, E.W., Stier, A.C., Silliman, B.R., 2011. The value of estuarine and coastal ecosystem services. *Ecological Monographs* 81, 169–193. <https://doi.org/10.1890/10-1510.1>
- Boar, R.R., Kirby, J.J.H., Leeming, D.J., 1999. Variations in the quality of the thatching reed *Phragmites australis* from wetlands in East Anglia, England. *Geological Society, London, Special Publications* 163, 145–151. <https://doi.org/10.1144/GSL.SP.1999.163.01.12>
- Bouma, T.J., De Vries, M.B., Low, E., Peralta, G., Tanczos, I.C., van de Koppel, J., Herman, P.M.J., 2005. Trade-offs Related to Ecosystem Engineering: A Case Study on Stiffness of Emerging Macrophytes. *Ecology* 86, 2187–2199. <https://doi.org/10.1890/04-1588>
- Cao, H., Zhu, Z., James, R., Herman, P.M.J., Zhang, L., Yuan, L., Bouma, T.J., 2020. Wave effects on seedling establishment of three pioneer marsh species: survival, morphology and biomechanics. *Annals of Botany* 125, 345–352. <https://doi.org/10.1093/aob/mcz136>
- Chatagnier, J., 2012. The biomechanics of salt marsh vegetation applied to wave and surge attenuation. Louisiana State University.
- Cho, J.-S., Lee, J.-S., Kim, J.-W., 2017. Distribution of *Phragmites australis* Communities with Different Habitat Salinity. *Journal of Coastal Research* 335, 1210–1216. <https://doi.org/10.2112/JCOASTRES-D-16-00065.1>
- Dalrymple, R.A., Kirby, J.T., Hwang, P.A., 1984. Wave Diffraction Due to Areas of Energy Dissipation. *Journal of Waterway, Port, Coastal, and Ocean Engineering* 110, 67–79. [https://doi.org/10.1061/\(ASCE\)0733-950X\(1984\)110:1\(67\)](https://doi.org/10.1061/(ASCE)0733-950X(1984)110:1(67))
- Duarte, C.M., Losada, I.J., Hendriks, I.E., Mazarrasa, I., Marbà, N., 2013. The role of coastal plant communities for climate change mitigation and adaptation. *Nature Clim Change* 3, 961–968.

- <https://doi.org/10.1038/nclimate1970>
- Elschot, K., Bouma, T.J., Temmerman, S., Bakker, J.P., 2013. Effects of long-term grazing on sediment deposition and salt-marsh accretion rates. *Estuarine, Coastal and Shelf Science* 133, 109–115. <https://doi.org/10.1016/j.ecss.2013.08.021>
- Etminan, V., Lowe, R.J., Ghisalberti, M., 2019. Canopy resistance on oscillatory flows. *Coastal Engineering* 152, 103502. <https://doi.org/10.1016/j.coastaleng.2019.04.014>
- Feagin, R.A., Irish, J.L., Möller, I., Williams, A.M., Colón-Rivera, R.J., Mousavi, M.E., 2011. Short communication: Engineering properties of wetland plants with application to wave attenuation. *Coastal Engineering* 58, 251–255. <https://doi.org/10.1016/j.coastaleng.2010.10.003>
- Foster-Martinez, M.R., Lacy, J.R., Ferner, M.C., Variano, E.A., 2018. Wave attenuation across a tidal marsh in San Francisco Bay. *Coastal Engineering* 136, 26–40. <https://doi.org/10.1016/j.coastaleng.2018.02.001>
- Garzon, J.L., Maza, M., Ferreira, C.M., Lara, J.L., Losada, I.J., 2019. Wave Attenuation by *Spartina* Saltmarshes in the Chesapeake Bay Under Storm Surge Conditions. *J. Geophys. Res. Oceans* 124, 5220–5243. <https://doi.org/10.1029/2018JC014865>
- Gijón Mancheño, A., Jansen, W., Uijttewaalt, W.S.J., Reniers, A.J.H.M., van Rooijen, A.A., Suzuki, T., Etminan, V., Winterwerp, J.C., 2021. Wave transmission and drag coefficients through dense cylinder arrays: Implications for designing structures for mangrove restoration. *Ecological Engineering* 165, 106231. <https://doi.org/10.1016/j.ecoleng.2021.106231>
- Goring, D.G., Nikora, V.I., 2002. Despiking Acoustic Doppler Velocimeter Data. *J. Hydraul. Eng.* 128, 117–126. [https://doi.org/10.1061/\(ASCE\)0733-9429\(2002\)128:1\(117\)](https://doi.org/10.1061/(ASCE)0733-9429(2002)128:1(117))
- Gosselin, F., De Langre, E., Machado-Almeida, B.A., 2010. Drag reduction of flexible plates by reconfiguration. *J. Fluid Mech.* 650, 319–341. <https://doi.org/10.1017/S0022112009993673>
- Heuner, M., Silinski, A., Schoelynck, J., Bouma, T.J., Puijalon, S., Troch, P., Fuchs, E., Schröder, B., Schröder, U., Meire, P., Temmerman, S., 2015. Ecosystem Engineering by Plants on Wave-Exposed Intertidal Flats Is Governed by Relationships between Effect and Response Traits. *PLoS ONE* 10, e0138086. <https://doi.org/10.1371/journal.pone.0138086>
- Hu, Z., Suzuki, T., Zitman, T., Uittewaalt, W., Stive, M., 2014. Laboratory study on wave dissipation by vegetation in combined current–wave flow. *Coastal Engineering* 88, 131–142. <https://doi.org/10.1016/j.coastaleng.2014.02.009>
- Jadhav, R.S., Chen, Q., 2013. Probability distribution of wave heights attenuated by salt marsh vegetation during tropical cyclone. *Coastal Engineering* 82, 47–55. <https://doi.org/10.1016/j.coastaleng.2013.08.006>
- Jalonen, J., Järvelä, J., 2013. Impact of Tree Scale on Drag: Experiments in a Towing tank, in: *Proceedings of 2013 IAHE World Congress*.
- Keulegan, G.H., Carpenter, L.H., 1958. Forces on cylinders and plates in an oscillating fluid. *J. RES. NATL. BUR. STAN.* 60, 423. <https://doi.org/10.6028/jres.060.043>
- Knutson, P.L., Brochu, R.A., Seeling, W.N., Margaret, I., 1982. Wave Damping in *Spartina Alterniflora* marsh. *Wetlands* 2, 87–104.
- Koftis, T., Prinos, P., Stratigaki, V., 2013. Wave damping over artificial *Posidonia oceanica* meadow: A large-scale experimental study. *Coastal Engineering* 73, 71–83. <https://doi.org/10.1016/j.coastaleng.2012.10.007>
- Lab, M. F. H. R. (2019). Storm Surges at the Eastern Shore of Virginia National Wildlife Refuge, HydroShare, <https://doi.org/10.4211/hs.51346939a66a45e5b7e4a33b48645a6c>
- Lara, J.L., Maza, M., Ondiviela, B., Trinogga, J., Losada, I.J., Bouma, T.J., Gordejuela, N., 2016. Large-scale 3-D experiments of wave and current interaction with real vegetation. Part 1: Guidelines for physical modeling. *Coastal Engineering* 107, 70–83. <https://doi.org/10.1016/j.coastaleng.2015.09.012>



- Lei, J., Nepf, H., 2019a. Wave damping by flexible vegetation: Connecting individual blade dynamics to the meadow scale. *Coastal Engineering* 147, 138–148. <https://doi.org/10.1016/j.coastaleng.2019.01.008>
- Lei, J., Nepf, H., 2019b. Blade dynamics in combined waves and current. *Journal of Fluids and Structures* 87, 137–149. <https://doi.org/doi:10.1016/j.jfluidstructs.2019.03.020>
- Li, H., Zhi, Y., An, S., Zhao, L., Zhou, C., Deng, Z., Gu, S., 2009. Density-dependent effects on the dieback of exotic species *Spartina anglica* in coastal China. *Ecological Engineering* 35, 544–552. <https://doi.org/10.1016/j.ecoleng.2008.03.001>
- Li, H., Lei, G., Zhi, Y., Bridgewater, P., Zhao, L., Wang, Y., Deng, Z., Liu, Y., Liu, F., An, S., 2011. Phenotypic responses of *Spartina anglica* to duration of tidal immersion. *Ecol Res* 26, 395–402. <https://doi.org/10.1007/s11284-010-0794-z>
- Lowe, R.J., Koseff, J.R., Monismith, S.G., 2005. Oscillatory flow through submerged canopies: 1. Velocity structure. *Journal of Geophysical Research: Oceans* 110. <https://doi.org/10.1029/2004JC002788>
- Losada, I.J., Maza, M., Lara, J.L., 2016. A new formulation for vegetation-induced damping under combined waves and currents. *Coastal Engineering* 107, 1–13. <https://doi.org/10.1016/j.coastaleng.2015.09.011>
- Luhar, M., Nepf, H.M., 2011. Flow-induced reconfiguration of buoyant and flexible aquatic vegetation. *Limnol. Oceanogr.* 56, 2003–2017. <https://doi.org/10.4319/lo.2011.56.6.2003>
- Luhar, M., 2012. Analytical and Experimental Studies of Plant-Flow Interaction at Multiple Scales. Massachusetts Institute of Technology. Woods Hole Oceanographic Institution.
- Luhar, M., Infantes, E., Nepf, H., 2017. Seagrass blade motion under waves and its impact on wave decay. *J. Geophys. Res. Oceans* 122, 3736–3752. <https://doi.org/10.1002/2017JC012731>
- Luhar, M., Nepf, H.M., 2016. Wave induced dynamics of flexible blades. *Journal of Fluids and Structures* 61, 20–41. <https://doi.org/10.1016/j.jfluidstructs.2015.11.007>
- Maricle, B.R., Koteyeva, N.K., Voznesenskaya, E.V., Thomasson, J.R., Edwards, G.E., 2009. Diversity in leaf anatomy, and stomatal distribution and conductance, between salt marsh and freshwater species in the C4 genus *Spartina* (Poaceae). *New Phytologist* 184, 216–233. <https://doi.org/10.1111/j.1469-8137.2009.02903.x>
- Maza, M., Lara, J.L., Losada, I.J., 2019. Experimental analysis of wave attenuation and drag forces in a realistic fringe *Rhizophora* mangrove forest. *Advances in Water Resources* 131, 103376. <https://doi.org/10.1016/j.advwatres.2019.07.006>
- Maza, M., Lara, J.L., Losada, I.J., Ondiviela, B., Trinogga, J., Bouma, T.J., 2015. Large-scale 3-D experiments of wave and current interaction with real vegetation. Part 2: Experimental analysis. *Coastal Engineering* 106, 73–86. <https://doi.org/10.1016/j.coastaleng.2015.09.010>
- McLeod, E., Chmura, G.L., Bouillon, S., Salm, R., Björk, M., Duarte, C.M., Lovelock, C.E., Schlesinger, W.H., Silliman, B.R., 2011. A blueprint for blue carbon: toward an improved understanding of the role of vegetated coastal habitats in sequestering CO<sub>2</sub>. *Frontiers in Ecology and the Environment* 9, 552–560. <https://doi.org/10.1890/110004>
- Mendez, F.J., Losada, I.J., 2004. An empirical model to estimate the propagation of random breaking and nonbreaking waves over vegetation fields. *Coastal Engineering* 51, 103–118. <https://doi.org/10.1016/j.coastaleng.2003.11.003>
- Moeller, I., Spencert, T., French, J.R., 1996. Wind Wave Attenuation over Saltmarsh Surfaces: Preliminary Results from Norfolk, England. *Journal of Coastal Research* 12, 1009–1016.
- Mullarney, J.C., Henderson, S.M., 2010. Wave-forced motion of submerged single-stem vegetation. *J. Geophys. Res.* 115, C12061. <https://doi.org/10.1029/2010JC006448>
- Nada, R.M., Khedr, A.H.A., Serag, M.S., El-Nagar, N.A., 2015. Growth, photosynthesis and stress-inducible genes of *Phragmites australis* (Cav.) Trin. ex Steudel from different habitats. *Aquatic*

- Botany 124, 54–62. <https://doi.org/10.1016/j.aquabot.2015.03.007>
- Nikora, V., Goring, D., 2000. Flow Turbulence over Fixed and Weakly Mobile Gravel Beds. *J. Hydraul. Eng.* 126, 679–690. [https://doi.org/10.1061/\(ASCE\)0733-9429\(2000\)126:9\(679\)](https://doi.org/10.1061/(ASCE)0733-9429(2000)126:9(679))
- Ostendorp, W., Möller, J., 1991. EM-algorithm as a tool for structure analysis of stands of the common reed (*Phragmites australis*). *Ecological Modelling* 53, 27–38. [https://doi.org/10.1016/0304-3800\(91\)90139-R](https://doi.org/10.1016/0304-3800(91)90139-R)
- Paul, M., Bouma, T., Amos, C., 2012. Wave attenuation by submerged vegetation: combining the effect of organism traits and tidal current. *Mar. Ecol. Prog. Ser.* 444, 31–41. <https://doi.org/10.3354/meps09489>
- Paul, M., Rupprecht, F., Möller, I., Bouma, T.J., Spencer, T., Kudella, M., Wolters, G., Wesenbeeck, B.K. van, Jensen, K., Miranda-Lange, M., Schimmels, S., 2016. Plant stiffness and biomass as drivers for drag forces under extreme wave loading: A flume study on mimics. *Coastal Engineering* 117, 70–78. <https://doi.org/10.1016/j.coastaleng.2016.07.004>
- Pendleton, L., Donato, D.C., Murray, B.C., Crooks, S., Jenkins, W.A., Sifleet, S., Craft, C., Fourqurean, J.W., Kauffman, J.B., Marbà, N., Megonigal, P., Pidgeon, E., Herr, D., Gordon, D., Baldera, A., 2012. Estimating Global “Blue Carbon” Emissions from Conversion and Degradation of Vegetated Coastal Ecosystems. *PLoS ONE* 7, e43542. <https://doi.org/10.1371/journal.pone.0043542>
- Rupprecht, F., 2015. Vegetation succession and coastal protection by wave dissipation in salt marshes of North-West Europe. Universität Hamburg.
- Rupprecht, F., Möller, I., Evans, B., Spencer, T., Jensen, K., 2015. Biophysical properties of salt marsh canopies — Quantifying plant stem flexibility and above ground biomass. *Coastal Engineering* 100, 48–57. <https://doi.org/10.1016/j.coastaleng.2015.03.009>
- Schaefer, R., 2019. Impacts and Vegetation-induced Attenuation of Wind-and Vessel-generated Waves. University of Delaware.
- Schoutens, K., Heuner, M., Fuchs, E., Minden, V., Schulte-Ostermann, T., Belliard, J.-P., Bouma, T.J., Temmerman, S., 2020. Nature-based shoreline protection by tidal marsh plants depends on trade-offs between avoidance and attenuation of hydrodynamic forces. *Estuarine, Coastal and Shelf Science* 236, 106645. <https://doi.org/10.1016/j.ecss.2020.106645>
- Schoutens, K., Heuner, M., Minden, V., Schulte Ostermann, T., Silinski, A., Belliard, J.-P., Temmerman, S., 2019. How effective are tidal marshes as nature-based shoreline protection throughout seasons. *Limnol. Oceanogr.* 64, 1750–1762. <https://doi.org/10.1002/lno.11149>
- Schulze, D., Rupprecht, F., Nolte, S., Jensen, K., 2019. Seasonal and spatial within-marsh differences of biophysical plant properties: implications for wave attenuation capacity of salt marshes. *Aquat Sci* 81, 65. <https://doi.org/10.1007/s00027-019-0660-1>
- Silinski, A., Heuner, M., Schoelynck, J., Puijalon, S., Schröder, U., Fuchs, E., Troch, P., Bouma, T.J., Meire, P., Temmerman, S., 2015. Effects of Wind Waves versus Ship Waves on Tidal Marsh Plants: A Flume Study on Different Life Stages of *Scirpus maritimus*. *PLoS ONE* 10, e0118687. <https://doi.org/10.1371/journal.pone.0118687>
- Sutton-Grier, A.E., Wowk, K., Bamford, H., 2015. Future of our coasts: The potential for natural and hybrid infrastructure to enhance the resilience of our coastal communities, economies and ecosystems. *Environmental Science & Policy* 51, 137–148. <https://doi.org/10.1016/j.envsci.2015.04.006>
- Tan, C., Huang, B., Liu, D., Qiu, J., Chen, H., Li, Y., Hu, Z., 2019. Effect of Mimic Vegetation with Different Stiffness on Regular Wave Propagation and Turbulence. *Water* 11, 109. <https://doi.org/10.3390/w11010109>
- Tinoco, R.O., San Juan, J.E., Mullarney, J.C., 2020. Simplification bias: lessons from laboratory and field experiments on flow through aquatic vegetation. *Earth Surf. Process. Landforms* 45, 121–143.



- https://doi.org/10.1002/esp.4743
- van Veelen, T.J., Fairchild, T.P., Reeve, D.E., Karunarathna, H., 2020. Experimental study on vegetation flexibility as control parameter for wave damping and velocity structure. *Coastal Engineering* 157, 103648. <https://doi.org/10.1016/j.coastaleng.2020.103648>
- van Veelen, T.J., Karunarathna, H., Reeve, D.E., 2021. Modelling wave attenuation by quasi-flexible coastal vegetation. *Coastal Engineering* 164, 103820. <https://doi.org/10.1016/j.coastaleng.2020.103820>
- Västilä, K., Järvelä, J., 2014. Modeling the flow resistance of woody vegetation using physically based properties of the foliage and stem. *Water Resour. Res.* 50, 229–245. <https://doi.org/10.1002/2013WR013819>
- Vuik, V., Jonkman, S.N., Borsje, B.W., Suzuki, T., 2016. Nature-based flood protection: The efficiency of vegetated foreshores for reducing wave loads on coastal dikes. *Coastal Engineering* 116, 42–56. <https://doi.org/10.1016/j.coastaleng.2016.06.001>
- Vuik, V., Suh Heo, H.Y., Zhu, Z., Borsje, B.W., Jonkman, S.N., 2018. Stem breakage of salt marsh vegetation under wave forcing: A field and model study. *Estuarine, Coastal and Shelf Science* 200, 41–58. <https://doi.org/10.1016/j.ecss.2017.09.028>
- Wan Yusof, K., Mujahid Muhammad, M., Raza Ul Mustafa, M., Azazi Zakaria, N., Gahani, A.Ab., 2017. Analysis of Manning's and Drag Coefficients for Flexible Submerged Vegetation. *IOP Conf. Ser.: Mater. Sci. Eng.* 216, 012046. <https://doi.org/10.1088/1757-899X/216/1/012046>
- Wang, X.Y., Xie, W.M., Zhang, D., He, Q., 2016. Wave and vegetation effects on flow and suspended sediment characteristics: A flume study. *Estuarine, Coastal and Shelf Science* 182, 1–11. <https://doi.org/10.1016/j.ecss.2016.09.009>
- Whittaker, P., Wilson, C., Aberle, J., Rauch, H.P., Xavier, P., 2013. A drag force model to incorporate the reconfiguration of full-scale riparian trees under hydrodynamic loading. *Journal of Hydraulic Research* 51, 569–580. <https://doi.org/10.1080/00221686.2013.822936>
- Wu, W., Ozeren, Y., Chen, Q., Jadhav, R., Wren, D., 2016. Laboratory and Field Investigations of Wave Attenuation by Live Marsh Vegetation 10.
- Xi, M., Kong, F., Li, Y., 2017. Temporal Variations in Growth and Aboveground Biomass of *Phragmites australis* and EVI Analysis in Jiaozhou Bay Coastal Salt Marshes, China. *Journal of Resources and Ecology* 8, 641–647. <https://doi.org/10.5814/j.issn.1674-764x.2017.06.011>
- Yang, S.L., Luo, X., Temmerman, S., Kirwan, M., Bouma, T., Xu, K., Zhang, S., Fan, J., Shi, B., Yang, H., Wang, Y.P., Shi, X., Gao, S., 2020. Role of delta-front erosion in sustaining salt marshes under sea-level rise and fluvial sediment decline: Role of delta-front erosion in sustaining marsh. *Limnol Oceanogr.* <https://doi.org/10.1002/lno.11432>
- Yang, S.L., Shi, B.W., Bouma, T.J., Ysebaert, T., Luo, X.X., 2012. Wave Attenuation at a Salt Marsh Margin: A Case Study of an Exposed Coast on the Yangtze Estuary. *Estuaries and Coasts* 35, 169–182. <https://doi.org/10.1007/s12237-011-9424-4>
- Ysebaert, T., Yang, S., Zhang, L., He, Q., Bouma, T.J., Herman, P.M.J., 2011. Wave Attenuation by Two Contrasting Ecosystem Engineering Salt Marsh Macrophytes in the Intertidal Pioneer Zone. *Wetlands* 31, 1043–1054. <https://doi.org/10.1007/s13157-011-0240-1>
- Zhang, X., Lin, P., Gong, Z., Li, B., Chen, X., 2020. Wave attenuation by *Spartina alterniflora* under macro-tidal and storm surge conditions. *Wetlands* 40, 2151–2162. <https://doi.org/10.1007/s13157-020-01346-w>
- Zhang, X., Nepf, H., 2021. Wave-induced reconfiguration of and drag on marsh plants. *Journal of Fluids and Structures* 100, 103192. <https://doi.org/10.1016/j.jfluidstructs.2020.103192>
- Zhang, X., Nepf, H., 2020. Flow-induced reconfiguration of aquatic plants, including the impact of leaf sheltering. *Limnology and Oceanography* 65, 2697–2712. <https://doi.org/10.1002/lno.11542>
- Zhi, Y., Li, H., An, S., Zhao, L., Zhou, C., Deng, Z., 2007. Inter-specific competition: *Spartina*

929 *alterniflora* is replacing *Spartina anglica* in coastal China. Estuarine, Coastal and Shelf Science  
930 74, 437–448. <https://doi.org/10.1016/j.ecss.2007.04.026>  
931 Zhu, Z., Vuik, V., Visser, P.J., Soens, T., van Wesenbeeck, B., van de Koppel, J., Jonkman, S.N.,  
932 Temmerman, S., Bouma, T.J., 2020. Historic storms and the hidden value of coastal wetlands for  
933 nature-based flood defence. Nat Sustain 3, 853–862. <https://doi.org/10.1038/s41893-020-0556-z>  
934

398 wide range of water depth, wave amplitude, and wave period. [Losada et al. \(2016\)](#) reported a wave  
399 decay coefficient  $\beta$  (Table 4 in their paper) based on fitting the measured wave amplitudes along  
400 the meadow (7 measurements for each case) using  $\frac{a_{w,x}}{a_{w,0}} = \frac{1}{1+\beta x}$ . Comparing to Eq. 12, this was

- A physics-based prediction for wave dissipation by flexible marsh plants with leaves was developed and validated with laboratory experiments.
- The dependence of wave dissipation on the wave parameters, including the water depth, wave amplitude, and wave period, were explored in detail with model predictions.
- The impact of plant properties, including the leaf and stem geometry and mechanical properties, on wave dissipation were revealed by systematic model predictions.

**Declaration of interests**

☒ The authors declare that they have no known competing financial interests or personal relationships that could have appeared to influence the work reported in this paper.

☐ The authors declare the following financial interests/personal relationships which may be considered as potential competing interests: